Clim Dyn (2017) 49:493–519
DOI 10.1007/s00382-016-3355-5

Projection of temperature and heat waves for Africa with an ensemble of CORDEX Regional Climate Models

Alessandro Dosio[1]

Received: 8 January 2016 / Accepted: 7 September 2016 / Published online: 17 September 2016

Abstract The most severe effects of global warning will be related to the frequency and severity of extreme events. We provide an analysis of projections of temperature and related extreme events for Africa based on a large ensemble of Regional Climate Models from the COordinated Regional climate Downscaling EXperiment (CORDEX). Results are presented not only by means of widely used indices but also with a recently developed Heat Wave Magnitude Index-daily (HWMId), which takes into account both heat wave duration and intensity. Results show that under RCP8.5, warming of more than 3.5 °C is projected in JFM over most of the continent, whereas in JAS temperatures over large part of Northern Africa, the Sahara and the Arabian peninsula are projected to increase up to 6 °C. Large increase in in the number of warm days (Tx90p) is found over sub equatorial Africa, with values up to more than 90 % in JAS, and more than 80 % in JFM over e.g., the gulf of Guinea, Central African Republic, South Sudan and Ethiopia. Changes in Tn90p (warm nights) are usually larger, with some models projecting Tn90p reaching 95 % starting from around 2060 even under RCP4.5 over the Gulf of Guinea and the Sahel. Results also show that the total length of heat spells projected to occur normally (i.e. once every 2 years) under RCP8.5 may be longer than those occurring once every 30 years under the lower emission scenario. By employing the recently developed HWMId index, it is possible to investigate the relationship between heat wave length ad intensity; in particular it is shown that very intense heat waves such as that occurring over the Horn of Africa may have values of HWMId larger than that of longer, but relatively weak, heat waves over West Africa.

Keywords Heat Waves · HWMId · Regional Climate Models · CORDEX-Africa · Extreme temperature statistics

1 Introduction

It is well known that the most severe effects of global warming will be related not only to a change in the mean climate, but especially to an increase in frequency and intensity of extreme events, such as floods, droughts and heat waves. Africa is one of the most vulnerable regions to weather and climate variability (IPCC 2007); for instance, in 2002 north-eastern Nigeria suffered one of the hottest and driest spells in living memory, with recorded temperatures above 50 °C and dozens of people dying as a results of the heat wave (http://news.bbc.co.uk/2/hi/africa/2038164.stm).

Although the IPCC Special Report on Managing the Risks of Extreme Events and Disasters to Advance Climate Change Adaptation (IPCC 2012) claimed a low to medium confidence in the observed change of maximum temperature and heat waves frequency in Africa, mainly due to insufficient evidence and lack of literature, some works by Alexander et al. (2006) and New et al. (2006) reported a significant increase, at regional level, in the temperatures of both warmest and coldest days, and in the duration and frequency of warm spells especially in South and West Africa. More recently, Donat et al. (2013) presented a global analysis of climate extreme indices based on station data since the beginning of the twentieth century: although the station density over Africa is very scarce, significant trends in the number of warm days and nights and duration of warm spells are

✉ Alessandro Dosio
alessandro.dosio@jrc.ec.europa.eu

[1] Space, Security and Migration Directorate, European Commission Joint Research Centre (JRC), Ispra (VA), Italy

reported for e.g. South Africa. Based on the same dataset and reanalysis data, a comprehensive analysis of climate extreme indices simulated by Global Circulation Models (GCMs) was reported by Sillmann et al. (2013a). On the basis of reanalysis dataset for the period 1979–2011, Fontaine et al. (2013) reported an increased occurrence of hot days and heat waves in Northern Africa, associated to specific atmospheric anomalies over Morocco and the Western Sahara.

Under global warming, the occurrence and intensity of extreme events, defined by IPCC (2012) as a value of a weather or climate variable above or below a threshold value near the upper or lower ends of the range of observed values, are expected to change, as reported by e.g. Tebaldi et al. (2006), Russo and Sterl (2011), Orlowsky and Seneviratne (2011), and Sillmann et al. (2013b). However, due to their low spatial resolution, GCMs are not able to resolve small-scale processes that are influenced by e.g. topographical details, coastlines, and land-surface heterogeneities. When using Regional Climate Models (RCMs) to dynamically downscale the projections of the global models, the GCMs' simulation skills are not always improved, especially for the general characteristics of the mean climatology; however added value is found especially in the fine scales and in the ability of RCM to simulate extreme events (e.g. Kim et al. 2002; Diallo et al. 2012; Paeth and Mannig 2012; Diaconescu and Laprise 2013; Crétat et al. 2013; Haensler et al. 2013; Laprise et al. 2013; Lee and Hong 2013; Lee et al. 2013; Buontempo et al. 2014; Giorgi et al. 2014; Dosio et al. 2015).

Studies based on RCMs specifically investigating temperature extreme events in Africa are relatively scarce, and usually focused only on specific regions: Lyon (2009) investigated the relationship between heat waves and droughts in South Africa, Nandozi et al. (2012) studied the projected increase in temperature over Uganda, Justino et al. (2013) analyzed the relationship between projected maximum temperature, precipitation and fire risk, and James et al. (2013) focused on the implication of climate change of central Africa rain forest.

In order to foster international collaboration to generate an ensemble of high-resolution historical and future climate projections, the World Climate Research Programme CORDEX (COordinated Regional climate Downscaling EXperiment) (Giorgi et al. 2009) selected Africa as the first target region of study. Many works have since then focused on the analysis of present day climatology (e.g. Nikulin et al. 2012; Endris et al. 2013; Kalognomou et al. 2013; Kim et al. 2014; Krähenmann et al. 2013; Gbobaniyi et al. 2014; Dosio et al. 2015) and future projections (Laprise et al. 2013; Teichmann et al. 2013; Giorgi et al. 2014; Buontempo et al. 2014; Mariotti et al. 2014; Dosio and Panitz 2015; Pinto et al. 2015; Diallo et al. 2016). However, all these studies focused mainly on precipitation and mean temperature, and only Giorgi et al. (2014) provided explicit projections of heat waves duration, although based on the results of a single RCM.

Here, for the first time to our knowledge, we provide an analysis of projections of temperature and related extreme events for Africa based on the results of a large ensemble of CORDEX RCMs. Since large uncertainty exists in the projected climate extremes (e.g. Perkins 2011) we particularly focus on the discrepancies between models' results. In addition, statistics for the heat waves are presented in terms of a recently developed Heat Wave Magnitude Index-daily (HWMId) (Russo et al. 2014, 2015), specifically designed to take into account both heat wave duration and intensity, thus enabling the quantification of the magnitude of heat waves across different time periods and regions.

The paper is structured as follows: Sect. 2 describes the data and the HWMId index; in Sect. 3 results are shown and discussed; concluding remarks are presented in Sect. 4.

2 Data and methods

2.1 Models' simulations

Modelled daily temperature data were obtained from the RCMs participating to the CORDEX activity, listed in Table 1. RCMs were used to downscale the results of GCMs participating to the Coupled Model Intercomparison Project Phase 5 (CMIP5) (Taylor et al. 2012) over a numerical domain covering the entire African continent (Fig. 1) at a resolution of 0.44 °. Historical runs, forced by observed natural and anthropogenic atmospheric composition, cover the period from 1950 until 2005, whereas the projections (2006–2100) are forced by two Representative Concentration Pathways (RCP) (Moss et al. 2010; Vuuren et al. 2011), namely, RCP4.5 and RCP8.5.

Although results for CORDEX-Africa simulations from several other RCMs have been recently published (e.g. Haensler et al. 2013; Laprise et al. 2013; Buontempo et al. 2014; Giorgi et al. 2014), they are not, to our knowledge, publicly available through the Earth System Grid Federation (ESGF) server, and, consequently, they are not used in this study.

The matrix of simulations is far from being exhaustive; for instance only one RCM (SMHI-RCA4) was used to downscale a large ensemble of GCMs, whereas two RCMs (DMI-HIRHAM5 and KNMI-RACMO2) downscaled only a single GCM. However, some qualitative analysis can be performed on e.g. the effect of the large scale forcing versus regional processes (comparing the simulations of CLM-com-CLCM48 and SMHI-RCA4 for the same four GCMs), or the impact of using different RCMs when downscaling the same GCM (ICHEC-EARTH).

Datasets of observed daily temperature for Africa are scarce, with large gaps in both spatial and temporal coverage (e.g. Donat et al. 2013); in order to take into account this uncertainty, both the ERA-Interim reanalysis from the European Centre for Medium-Range Weather Forecasts (Dee et al. 2011) and the NCEP-DOE Reanalysis-2 (NCEP-2) (Kanamitsu et al. 2002) are used to evaluate models' results over the reference period (1981–2010). Both Sillmann et al. (2013a) and Donat et al. (2014) compared indices of temperature extremes from a range of gridded observations and reanalyses; they found that on average ERA-Interim performed closest to the observational datasets in regions where sufficiently complete observations were available, although local trends between different reanalyses may differ especially in areas where data are scarce.

2.2 Heat Wave Magnitude Index-daily (HWMId).

The definition of a heat wave is very broad, although it generally refers to a period of consecutive days where conditions are excessively hotter than normal (Perkins et al. 2012). Most of the widely used extreme temperature indices take into account only one single aspect (i.e., maximum temperature, duration, or frequency) during a defined period, which is not necessarily part of a heat spell, as pointed out by e.g., Perkins and Alexander (2013). Absolute threshold based indices (when maximum temperatures is e.g. 5 °C or more above the average for a reference period) do not yield comparable results for different geographical locations (Radinović and Ćurić 2012), and they are therefore of limited robustness (Alexander et al. 2006; Orlowsky and Seneviratne 2011; Russo and Sterl 2011; Perkins and Alexander 2013). Even percentile based indices such as the Warm Spell Duration Index (WSDI), specifically defined for detecting heat spells, considers only the duration of a heat wave: as a result, two heat waves of the same length are considered equally severe, even if all the days of one have higher temperatures than the other (Russo et al. 2014).

Here we use the recently developed Heat Wave Magnitude Index-daily (HWMId) (Russo et al. 2015) designed to take into account both heat wave duration and intensity. A thorough description of the HWMId, including its calculation, evaluation and comparison to other temperature indices is provided in Russo et al. (2015); consequently, only a synthetic description of its calculation is reported here.

The HWMId is defined as the maximum magnitude of the heatwaves in a year, where a heatwave is defined as the period of at least three consecutive days with maximum temperature above the daily threshold for the reference period. The threshold is defined as the 90-th percentile of daily maximum temperature, centered on a 31-day window. The magnitude of a heatwave is defined as the sum of the daily magnitude M_d of all the consecutive days composing an heatwave, and it is calculated as follows:

$$M_d(T_d) = \begin{cases} \frac{T_d - T_{30y25p}}{T_{30y75p} - T_{30y25p}}; & T_d > T_{30y25p} \\ 0; & T\_d \leq T_{30y25p} \end{cases} \quad (1)$$

Here, T_d is the daily maximum temperature, and T_{30y25p} and T_{30y75p} are the 25-th and 75-th percentiles of the yearly maximum temperatures over the reference period (1981–2010). The interquantile range $T_{30y75p} - T_{30y25p}$ defines the heatwave daily magnitude unit: as a consequence, a daily magnitude $M_d(T_d)$ equal to n indicates that the temperature anomaly on the day d with respect to T_{30yp25} is n times the climatological interquantile range (Russo et al. 2015).

3 Results

We first analyze present climate (1981–2010) seasonal climatology of daily mean, maximum (Tx), and minimum (Tn) temperature, and, subsequently, its future change (2071–2100) under different RCPs. The evaluation of models' results over present climate is performed not only for the RCMs, but also for the corresponding driving GCMs, in order to investigate whether downscaling is able to add value to the performances of the global models. For the model runs, the present climate period is defined by combining the model results of the historical simulations (1981–2005) with the first five years of the projection runs (2006–2010) under RCP4.5 (results using the first five years of the RCP8.5 runs are very similar).

Two percentile-based indices from the Expert Team on Climate Change Detection and Indices (ETCCDI) (e.g. Sillmann et al. 2013a) have been calculated, namely, Tx90p (warm days) i.e., the percentage of days in a season with Tx higher than he reference (1981–2010) 90-th percentile, and Tn90p (warm nights) i.e., the percentage of days in a season with Tn higher than the reference 90-th percentile.

In addition, the Warm Spell Duration Index (WSDI) is calculated, defined as the total number of days per year when, in intervals of at least three consecutive days, Tx is higher than the calendar 90-th percentile of the reference period. The three consecutive day threshold has been chosen to be consistent (and comparable) with the definition of heatwave in the calculation of the HWMId index. In addition, as the 90-th percentile is computed over the same period as that used for the evaluation of the present-day heatwave statistics (1981–2010), the choice of a longer heatwave threshold may result in a very small number of events.

Some of the analysis is performed over sub-regions defined as in the CORDEX protocol (see Fig. 1, and http://

www.smhi.se/forskning/forskningsomraden/klimatforskning/1.11299) and used in previous single- and multi-model evaluation studies over CORDEX-Africa (e.g Nikulin et al. 2012; Laprise et al. 2013). Following the same protocol, seasonal statistics are calculated for boreal winter, defined as January–February–March (JFM), and summer (July–August–September—JAS). On the other hand, heat waves indices are calculated on annual basis.

3.1 Temperature climatology

Figure 2 shows maps of models' ensemble median and median absolute deviation (MAD) of seasonal mean temperature. Results for the reference period (1981–2010) are compared with both ERA-Interim and NCEP-2 reanalyses. Tabbed values are reported in Table 2.

The RCMs' ability to reproduce present climate surface temperature has been extensively assessed in the past, and it will not be repeated here extensively. However it is worth noting that contrary to the ERA-interim driven RCM simulations, where a large multi-RCM ensemble has been evaluated, (Kim et al. 2014), for the GCM-downscaled runs only single-RCM studies are available (Laprise et al. 2013; Teichmann et al. 2013; Buontempo et al. 2014; Coppola et al. 2014; Dosio et al. 2015). An analysis of the performances of the GCMs can be found in e.g. Sillmann et al. (2013a) and Brands et al. (2013): RCMs' results are affected by the bias inherited through the lateral boundary conditions, in addition to those introduced by the RCM by means, for instance, of model errors and parameterizations.

Although differences up to nearly 2.5 °C exists amongst ERA-Interim and NCEP-2, RCMs' results are, in median, colder than both reanalyses over the Sahel and the Atlas Mountain in DJF, over EA especially in JAS and over South Africa in both seasons (Table 2). On the other hand, RCMs temperature is overestimated over central Africa especially

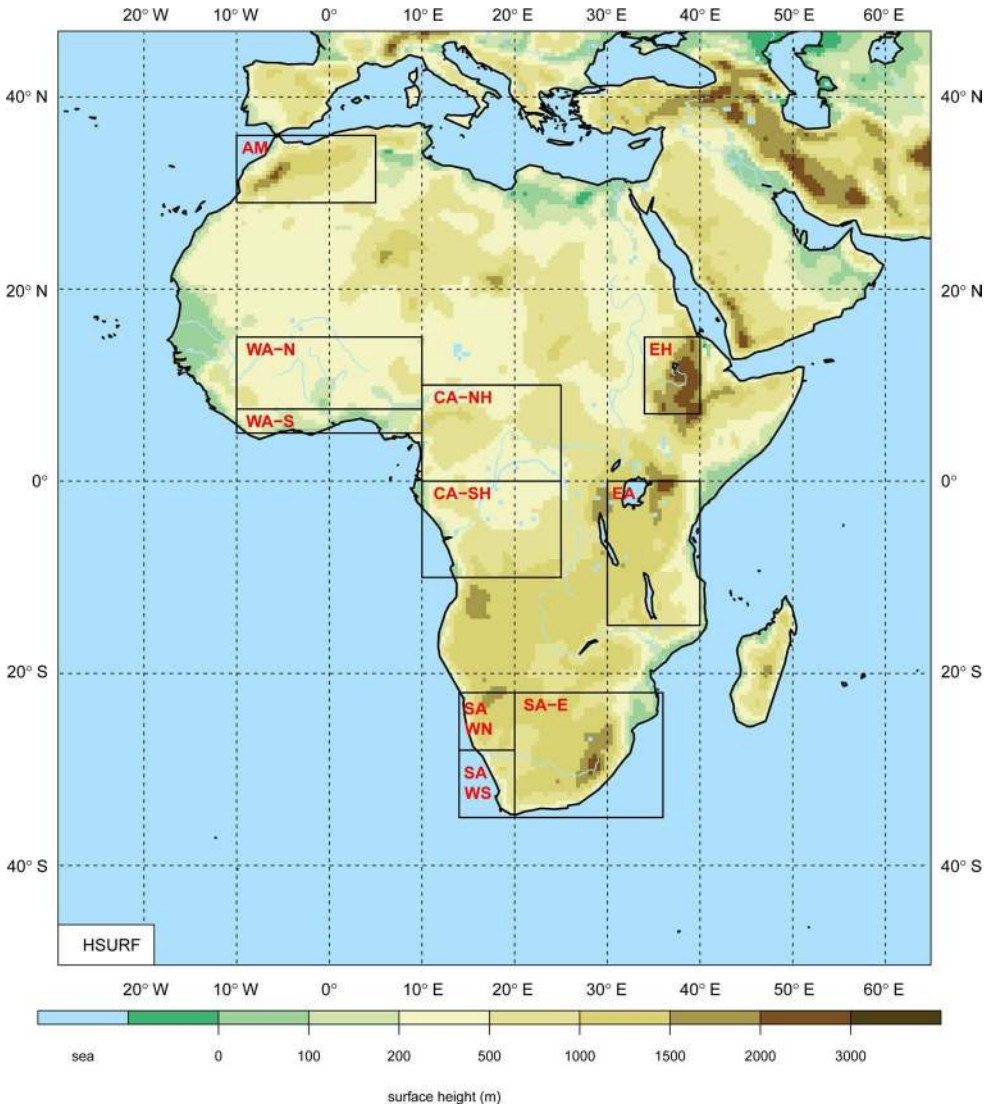

Fig. 1 Model domain and topography (m) of the CORDEX Africa simulations. Also shown are the evaluation regions as defined in http://www.smhi.se/forskning/forskningsomraden/klimatforskning/1.11299)

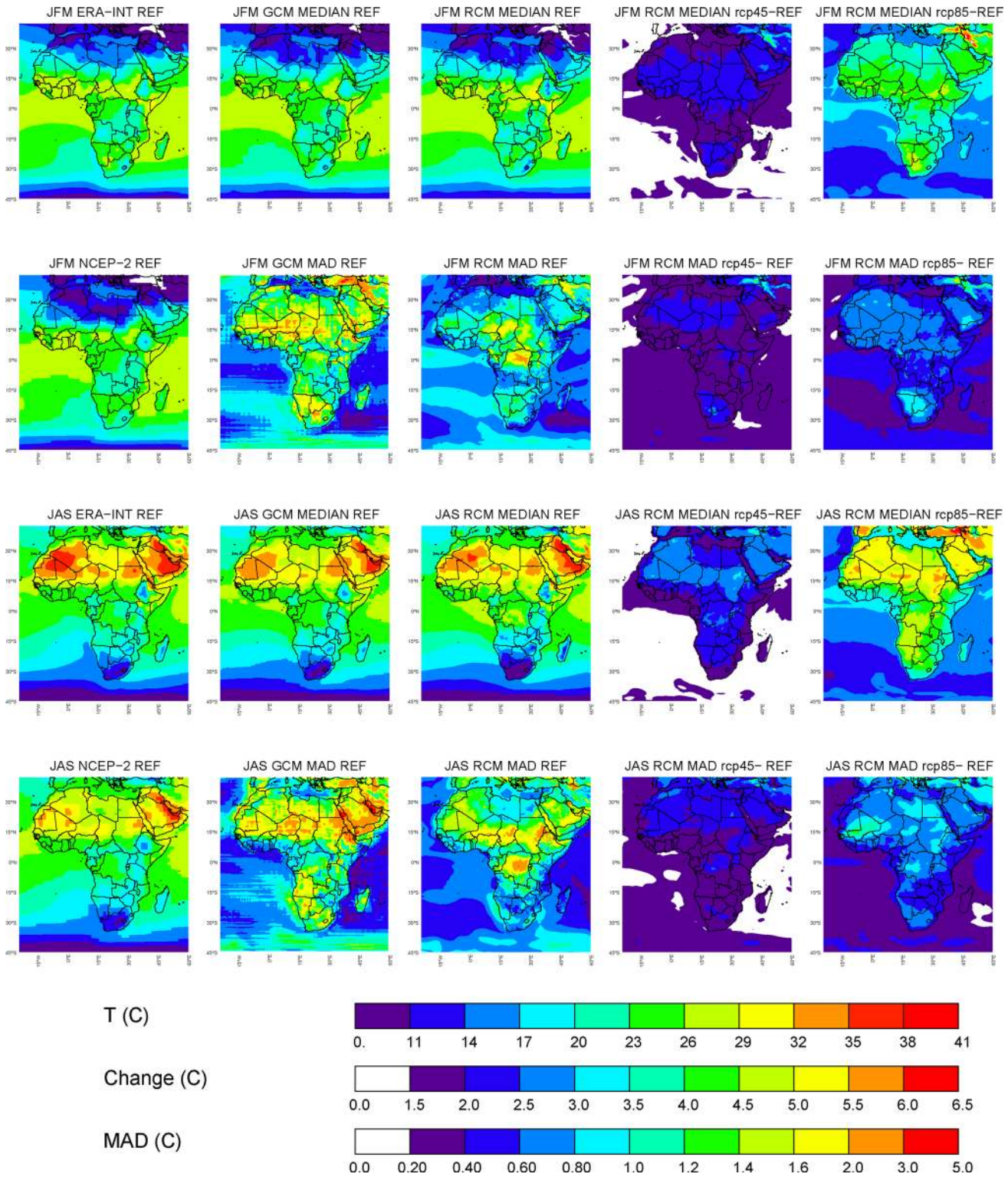

Fig. 2 Maps of seasonal mean temperature for austral (JFM) and boreal (JAS) summer, shown as models' ensemble median and inter-model variability (MAD). *First columns* show data from ERA-Interim and NCEP-2 reanalysis; *second* and *third column* shows GCMs and RCMs results for the reference climate (1981–2010) respectively; fourth and fifth columns show RCMs' projected climate change signal (i.e. 2071–2100 minus reference period) under RCP4.5 and RCP8.5 scenarios, respectively

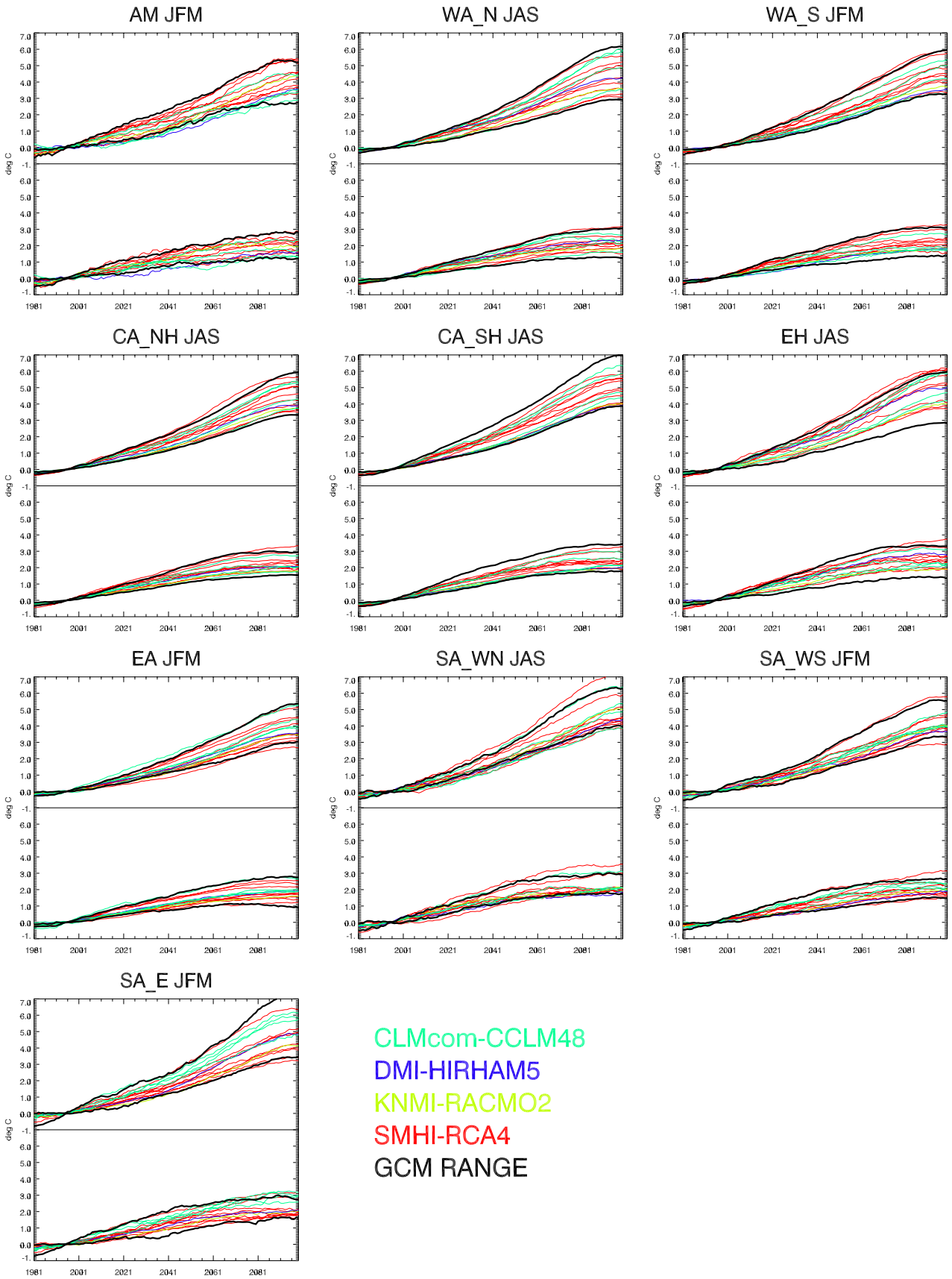
AM JFM
WA_N JAS
WA_S JFM
CA_NH JAS
CA_SH JAS
EH JAS
EA JFM
SA_WN JAS
SA_WS JFM
SA_E JFM
deg C
1981
2001
2021
2041
2061
2081
CLMcom-CCLM48
DMI-HIRHAM5
KNMI-RACMO2
SMHI-RCA4
GCM RANGE

◂**Fig. 3** Time evolution of seasonal mean temperature anomaly for the evaluation regions. All RCMs runs are shown; for CLMcom-CCLM-48 and SMHI-RCA4 the various lines (with the same color) correspond to runs with different forcing GCMs. The GCMs' range (maximum and minimum) is also shown (*black lines*). Note that the selected season is dependent on the region analysed

in JAS. Comparing RCMs' results to those of the driving GCMs' ones is not straightforward, as there are regions where RCMs results' are, in median, better than the GCMs' ones (e.g. WA_N, WA_S and EH, especially in JAS), whereas the opposite is true especially over South Africa.

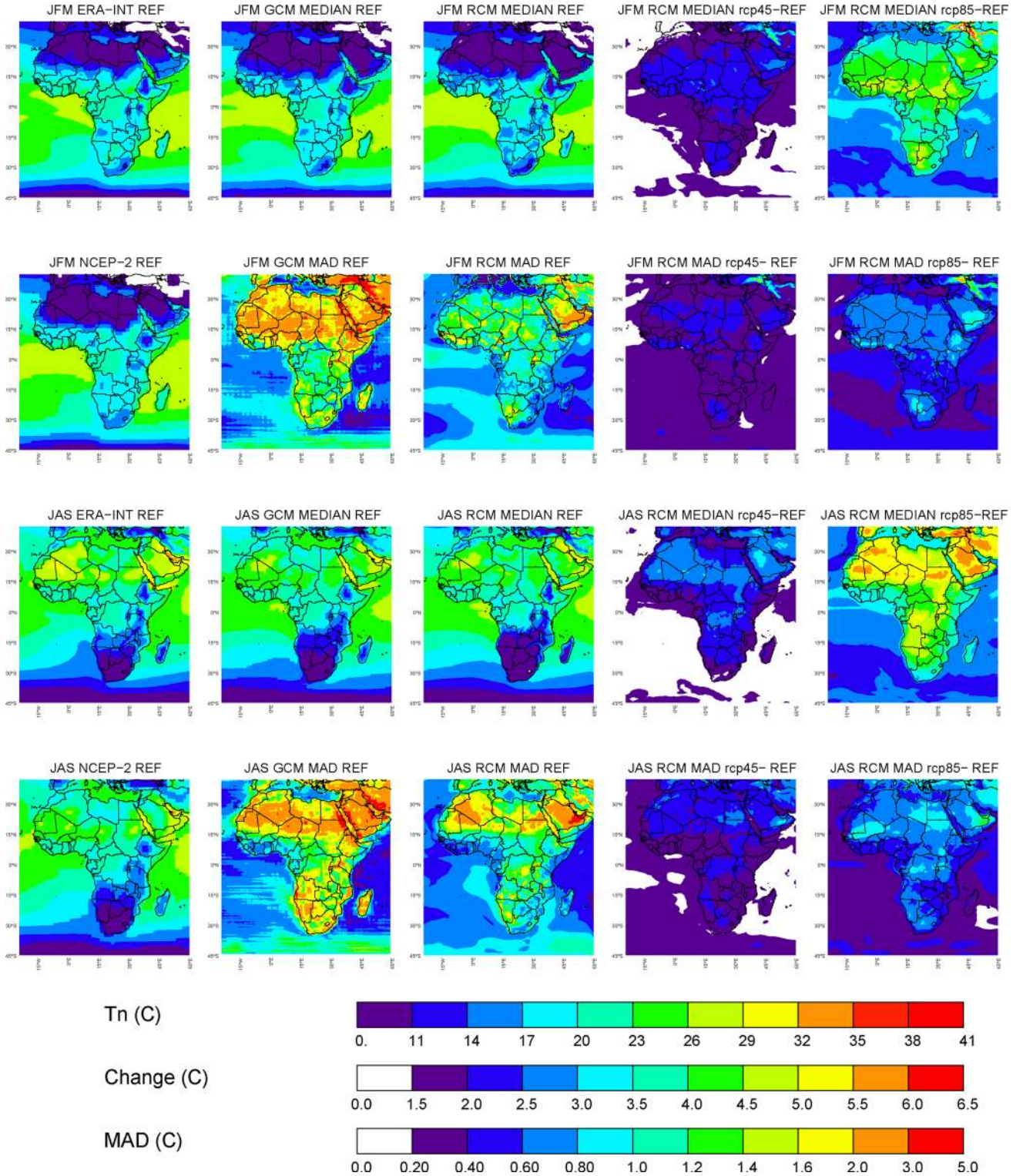

Fig. 4 As Fig. 2 but for seasonal minimum temperature

Table 1 Matrix of model simulations used in this study

GCM RCM	CLMcom-CCLM48	DMI-HIRHAM5	KNMI-RACMO2	SMHI-RCA4
ICHEC-EC-EARTH	X	X	X	X
MOHC-HadGEM2-ES	X			X
CNRM-CERFACS-CNRM-CM5	X			X
MPI-M-MPI-ESM-LR	X			X
CCma-CanESM2				X
MIROC-MIRCO5				X
NCC-NorESM1-M				X
IPSL-IPSL-CM5A-MR				X
NOAA-GFDL-GFDL-ESM2M				X

Four different RCMs (CLMcom-CCLM48, DMI-HIRHAM5, KNMI-RACMO2, SMHI-RCA4) were used to downscale the results of several GCMs participating to CMIP5. SMHI-RCA4 was used to downscale nine different GCMs, and CLMcom-CCLM48 four GCMs

Table 2 Values of seasonal mean temperature for selected regions over the present climate (1981–2010)

		NCEP-2	ERA-Interim	RCMs	GCMs
AM	JFM	11.12	12.69	10.37 (0.93)	11.18 (1.20)
	JAS	28.25	30.62	28.94 (1.36)	28.27 (1.15)
WA_N	JFM	26.11	27.22	25.27 (1.02)	25.06 (1.28)
	JAS	25.48	25.80	25.68 (1.25)	26.25 (1.07)
WA_S	JFM	26.50	26.74	26.38 (0.89)	25.95 (1.02)
	JAS	23.35	23.93	23.85 (0.90)	24.27 (0.68)
CA_NH	JFM	24.50	25.40	25.59 (1.25)	24.64 (0.94)
	JAS	22.61	23.04	23.86 (1.23)	23.81 (0.91)
CA_SH	JFM	23.18	22.71	23.15 (0.89)	23.52 (1.03)
	JAS	22.95	22.86	23.74 (1.33)	23.91 (1.17)
EH	JFM	22.10	22.39	22.14 (0.99)	22.05 (0.83)
	JAS	20.77	20.68	20.91 (1.67)	21.95 (1.28)
EA	JFM	22.56	22.55	22.04 (0.79)	22.75 (0.84)
	JAS	20.79	21.04	19.02 (0.78)	20.37 (0.87)
SA_WN	JFM	24.01	24.88	22.60 (1.08)	24.22 (1.41)
	JAS	14.97	15.85	12.37 (0.99)	15.44 (1.47)
SA_WS	JFM	22.29	23.48	22.47 (0.96)	24.16 (1.10)
	JAS	13.14	13.56	10.44 (0.97)	13.18 (1.20)
SA_E	JFM	24.45	24.81	22.65 (1.09)	23.34 (1.59)
	JAS	14.98	15.57	12.71 (0.76)	14.77 (1.24)

Values are reported as ensemble median and MAD (in brackets) of RCMs and GCMs. Values from ERA-Interim and NCEP-2 are also reported. Units are degrees Celsius

Dosio et al. (2015) showed that RCMs are not always able to improve the results of the driving GCMs, although when CLMcom-CCLM48 results were compared to those of the four driving GCMs, added value was found over the Sahara and South Africa, both in JFM and JAS.

The most striking difference between the results of global and regional models is the value of the inter-model variability (MAD), which shows generally lower values for the RCMs, a part for the Democratic Republic of Congo, where RCMs' MAD can reach, locally, vales up to 3 °C. This is in agreement with the results of Dosio and Panitz (2015), who showed that CLMcom-CCLM48 present-day mean temperature and daily ranges do not vary significantly with the different boundary conditions (despite the GCM values varying considerably), being on the contrary greatly influenced by local processes such as the land atmosphere interaction and feedback.

RCMs' future projections under the RCP4.5 scenario show,in median, a general temperature increase of around 2 °C over the whole continent in JFM, whereas in JAS a more pronounced warming (up to 3 °C) is found over north-equatorial Africa and the Arabian peninsula. Under the more severe RCP8.5 scenario, warming in JFM reaches 5 °C over South Africa, Chad, Central African Republic and South Sudan, whereas in JAS temperatures over large part of Northern Africa, the Sahara and the Arabian peninsula are projected to increase up to 6 °C. The inter model variability as expressed by the MAD is generally small for the RCP4.5 runs, whereas values of MAD up to 1 ° are found in JFM over South Africa. In JAS larger uncertainty is found especially over the Sahel, with values of MAD reaching 1.6 °C.

In order to investigate further the impact of inter-model variability on the projections, Fig. 3 shows the temporal evolution of temperature anomaly (with respect to the reference period) for selected sub-regions shown in Fig. 1. We first note the at the end of the Century, under RCP8.5, the uncertainty range (i.e maximum minus minimum) in the projected temperature anomalies can reach very large values, up to e.g. 3 °C over SA_WN in JAS. The RCMs' spread is generally in good agreement with the GCM's one, a part for local exceptions such as SA_WN, where one of the SMHI-RCA4 runs lies outside the GCM's range. In some

cases, (EH, CA_SH, and SA_E) the downscaling reduces the GCMs' uncertainty in the projected warming of around 1 °C. Second we note that the ranges of anomalies related to the two RCP scenarios may overlap, such as in WA_N in JAS, thus indicating that the uncertainty due to inter-model variability can be as large as that related to the choice of

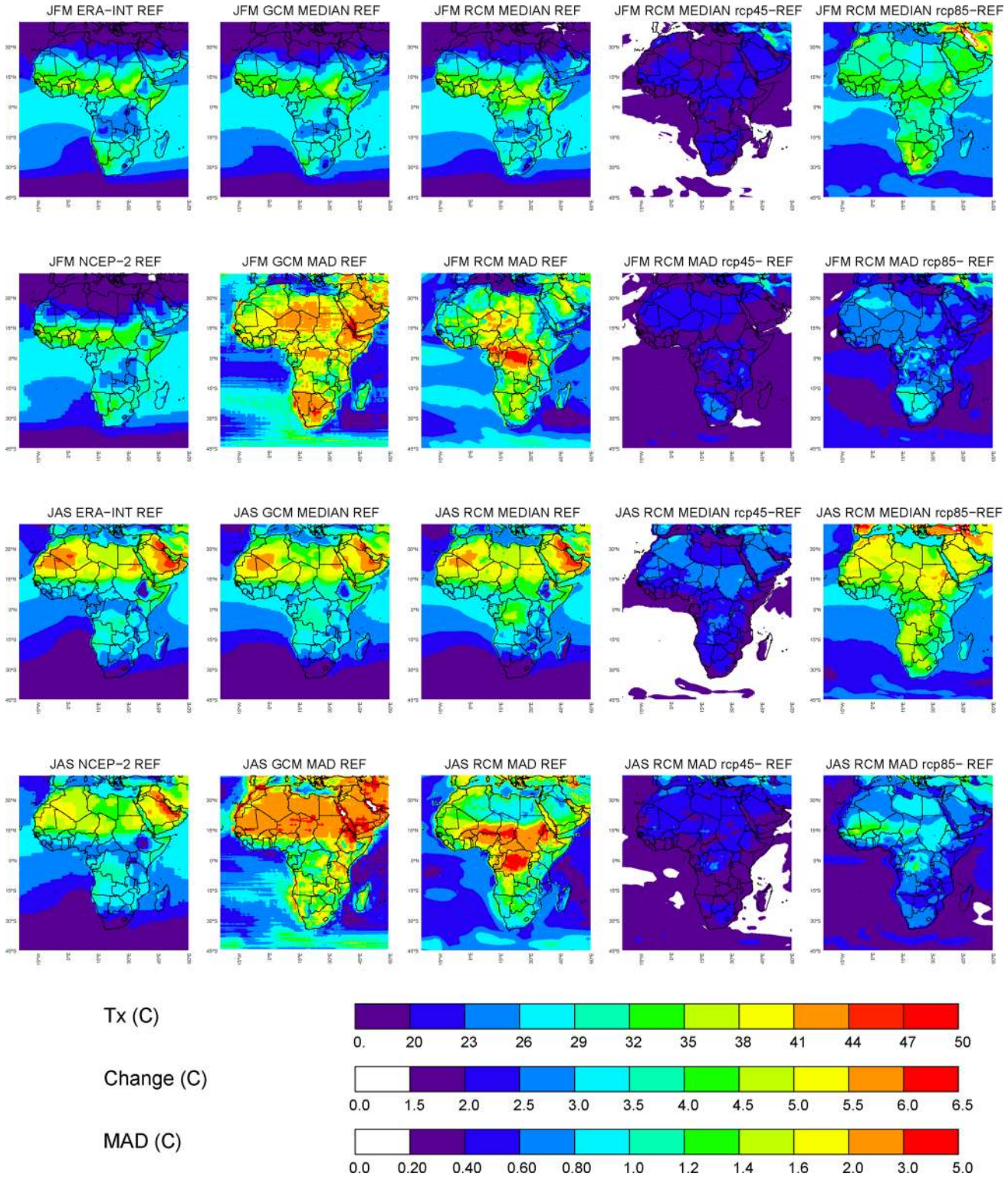

Fig. 5 As Fig. 2 but for seasonal maximum temperature

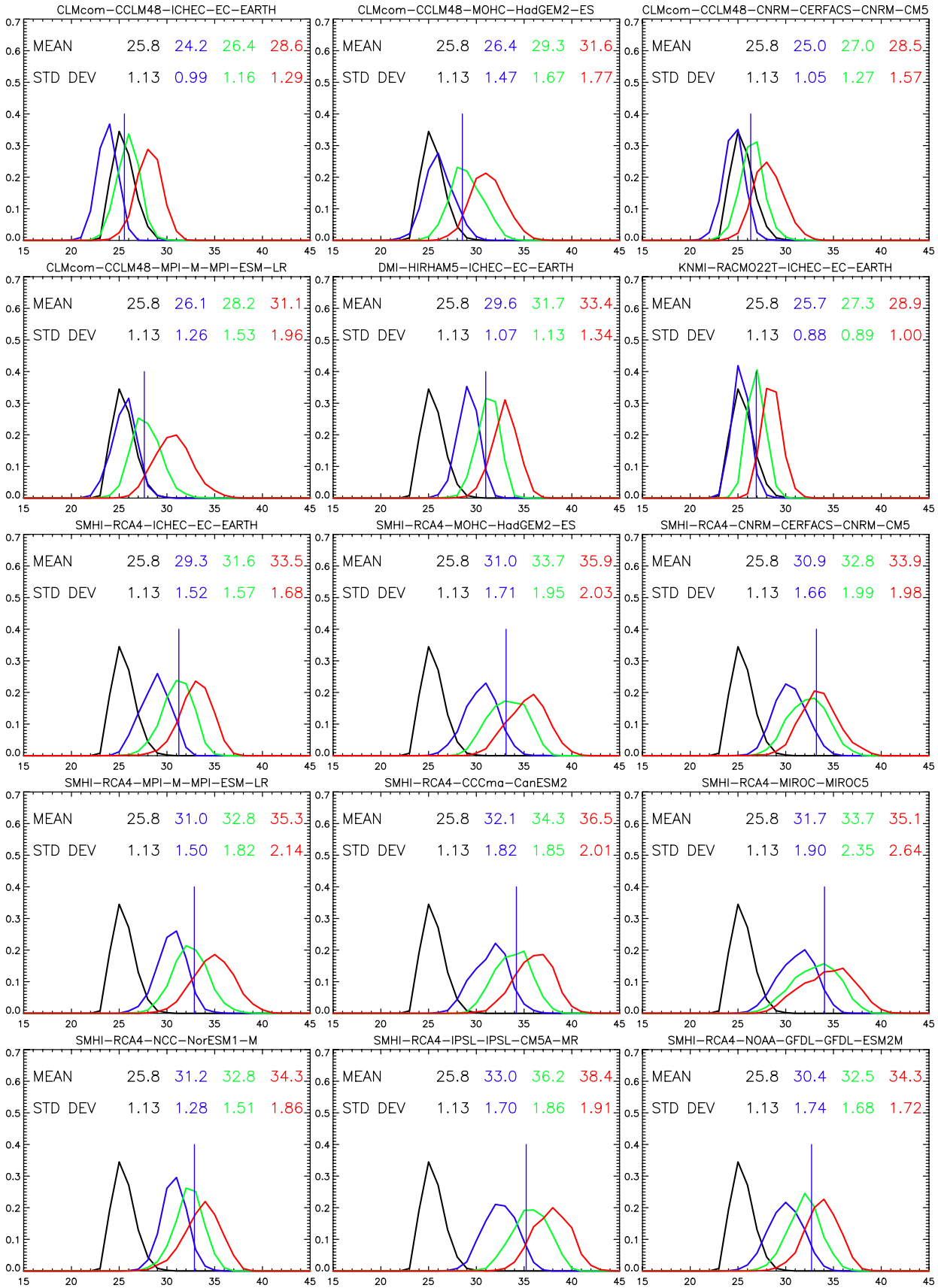
CLMcom−CCLM48−ICHEC−EC−EARTH
MEAN 25.8 24.2 26.4 28.6
STD DEV 1.13 0.99 1.16 1.29
CLMcom−CCLM48−MOHC−HadGEM2−ES
MEAN 25.8 26.4 29.3 31.6
STD DEV 1.13 1.47 1.67 1.77
CLMcom−CCLM48−CNRM−CERFACS−CNRM−CM5
MEAN 25.8 25.0 27.0 28.5
STD DEV 1.13 1.05 1.27 1.57
CLMcom−CCLM48−MPI−M−MPI−ESM−LR
MEAN 25.8 26.1 28.2 31.1
STD DEV 1.13 1.26 1.53 1.96
DMI−HIRHAM5−ICHEC−EC−EARTH
MEAN 25.8 29.6 31.7 33.4
STD DEV 1.13 1.07 1.13 1.34
KNMI−RACMO22T−ICHEC−EC−EARTH
MEAN 25.8 25.7 27.3 28.9
STD DEV 1.13 0.88 0.89 1.00
SMHI−RCA4−ICHEC−EC−EARTH
MEAN 25.8 29.3 31.6 33.5
STD DEV 1.13 1.52 1.57 1.68
SMHI−RCA4−MOHC−HadGEM2−ES
MEAN 25.8 31.0 33.7 35.9
STD DEV 1.13 1.71 1.95 2.03
SMHI−RCA4−CNRM−CERFACS−CNRM−CM5
MEAN 25.8 30.9 32.8 33.9
STD DEV 1.13 1.66 1.99 1.98
SMHI−RCA4−MPI−M−MPI−ESM−LR
MEAN 25.8 31.0 32.8 35.3
STD DEV 1.13 1.50 1.82 2.14
SMHI−RCA4−CCCma−CanESM2
MEAN 25.8 32.1 34.3 36.5
STD DEV 1.13 1.82 1.85 2.01
SMHI−RCA4−MIROC−MIROC5
MEAN 25.8 31.7 33.7 35.1
STD DEV 1.13 1.90 2.35 2.64
SMHI−RCA4−NCC−NorESM1−M
MEAN 25.8 31.2 32.8 34.3
STD DEV 1.13 1.28 1.51 1.86
SMHI−RCA4−IPSL−IPSL−CM5A−MR
MEAN 25.8 33.0 36.2 38.4
STD DEV 1.13 1.70 1.86 1.91
SMHI−RCA4−NOAA−GFDL−GFDL−ESM2M
MEAN 25.8 30.4 32.5 34.3
STD DEV 1.13 1.74 1.68 1.72

◂**Fig. 6** Probability Distribution Function of daily maximum temperature in JAS for CA_NH as modelled by the RCMs for the historical (1981–2010; *blue line*) and future (2071–2100) climate under RCP4.5 (*green line*) and RCP8.5 (*red line*) scenarios. The *black line* is the PDF of maximum temperature from ERA-Interim reanalysis. In each panel, the two lines of numbers indicate the observed (*black*), historical (*blue*) and projected (*green* and *red*) values of the mean and standard deviation, respectively. The *vertical blue line* represents the modelled historical 90th percentile of Tx. Units are degrees Celsius

the emission scenario. Finally, there are areas where the variability of projected anomalies strongly depends on the RCM, such as in SA_E in JFM. This aspect is investigated further by analyzing the results of each single GCM-RCM run separately, for three of the most significant cases.

For AM in JFM (Table 3), it is clear that the choice of RCM has a great influence on the projected temperature change; for instance, the three overall coldest and warmest projections are those of CLMcom-CCLM48 and SMHI-RCA4, respectively. In addition, when downscaling the same four GCMs, all CLMcom-CCLM48 anomalies are smaller than the SMHI-RCA4 ones, although the intra-model spread (δ = maximum − minimum) is very similar, being 1.84 °C for CLMcom-CCLM48 and 1.86 °C for SMHI-RCA4. For only one GCM (ICHEC-EARTH) downscaled results are available for all RCMs: in this case KNMI-RACMO2 shows the largest warming (3.87 °C). Considering that, in the case of SMHI-RCA4, all the warmest runs (except for the MOHC-HadGEM2-ESM) are those corresponding to GCMs that have not been downscaled by the other RCMs, one can only speculate whether, for instance, KNMI-RACMO2 would project the largest warming if it was used with more GCMs.

For CA_SH in JAS (Table 4), CLMcom-CCLM48 and SMHI-RCA4 give relatively close results, when the same GCMs are downscaled, with similar values of both mean and Delta. On the contrary, both DMI-HIRHAM45 and KNMI-RACMO2 project a smaller temperature increase than either CLMcom-CCLM48 or SMHI-RCA4: again, it would be interesting to investigate how much the inter-model variability would increase if these RCMs were used to downscale, for instance, the GCM that shows the smallest regional warming, namely CNRM-CERFACS-CNRM-CM5.

As last example, we investigate the projected temperature increase over SA_E in JAS (Table 5). In this case, SMHI-RCA4 shows both the largest and the smallest values, being 2.97 and 5.98 °C, respectively, but these results correspond to GCMs that have not been downscaled by other RCMs. When the same GCMs are compared, SMHI-RCA4 is systematically less warm than CLMcom-CCLM48; not only the mean value for SMHI-RCA4 (4.02 °C) is smaller than that of CLMcom-CCLM48 (5.17 °C), but so is the value of the intra-model spread (0.91 °C compared to 1.34 °C), showing that SMHI-RCA4 in this case is less sensitive than CLMcom-CCLM48 to forcing boundary conditions.

Figures 4 and 5 show maps of the ensemble median and MAD of seasonal minimum (Tn) and maximum (Tx) temperature, respectively. RCMs' results are generally similar to the GCMs' ones, and closer to ERA-Interim than NCEP-2. However, Tx is generally overestimated over central Africa, compared to ERA-Interim, both in JFM and JAS, as for mean temperature (Fig. 2). RCMs' intermodel variability is usually smaller than for the GCMs; however, MAD for Tx is greater than 3 °C over central Africa and part of the Sahara in JFM, and over most of north-equatorial Africa up to around 20 °N in JAS. On the contrary, RCMs' MAD for Tn shows relatively small values (less than 1.6 °C) in JFM but larger values over the Sahara, Northern Africa and the Arabian peninsula in JAS. Kim et al. (2014) also noted a large variability in the performances of the (ERA-interim) driven RCM simulations, with the skill of individual RCMs varying depending on the variable. Krähenmann et al. (2013) performed a detailed analysis of the performance of CLMcom-CCLM48 driven by ERA-Interim in simulating statistics of daily Tx and Tn: they found a considerable overestimation of the diurnal temperature range over the tropics due to a large warm bias in Tx, but a general underestimation of the diurnal range over the Sahara; these biases are claimed to be related to uncertainty in the cloud cover parameterization and soil thermal conductivity.

Maximum temperature is projected to increase by the RCMs, in general, similarly to the mean temperature, although some differences exist over the Sahel in JAS for both the ensemble median increase and the MAD (compare Figs. 2 and 5). Larger discrepancies are evident for Tn, especially under RCP8.5, with the projected warming being larger than that of mean temperature over north tropical Africa in JFM and over the Sahara, the Arabian peninsula and central Africa in JAS.

3.2 Probability Distribution function and Indices of extreme events

As the future occurrence of extreme events is related to both the shift in the mean and the change in the variability, it is important to investigate how climate models reproduce not only the temperature probability distribution function (PDF) in present climate condition, but also its change under

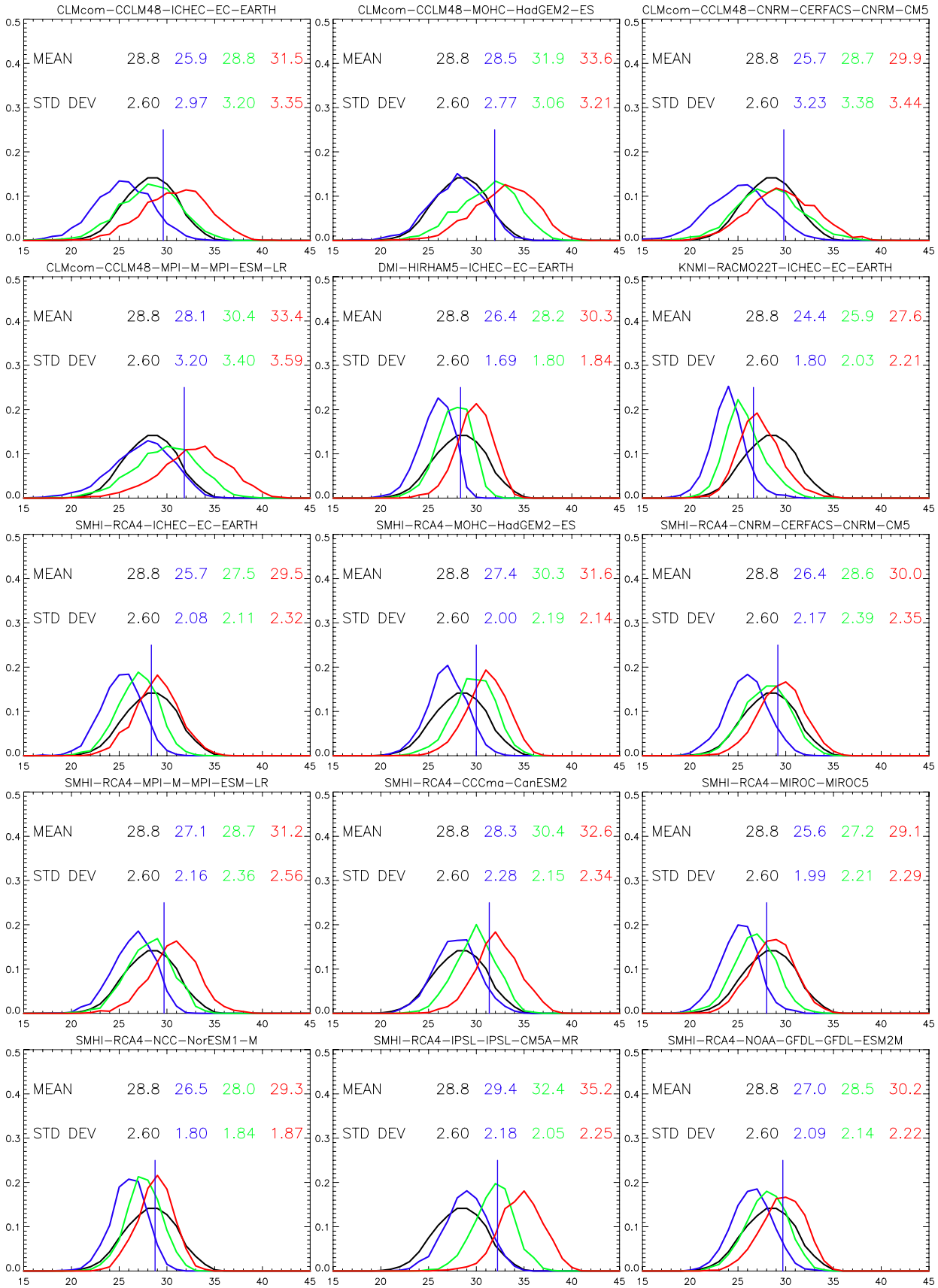

Fig. 7 As Fig. 6 but for SA_E in JFM

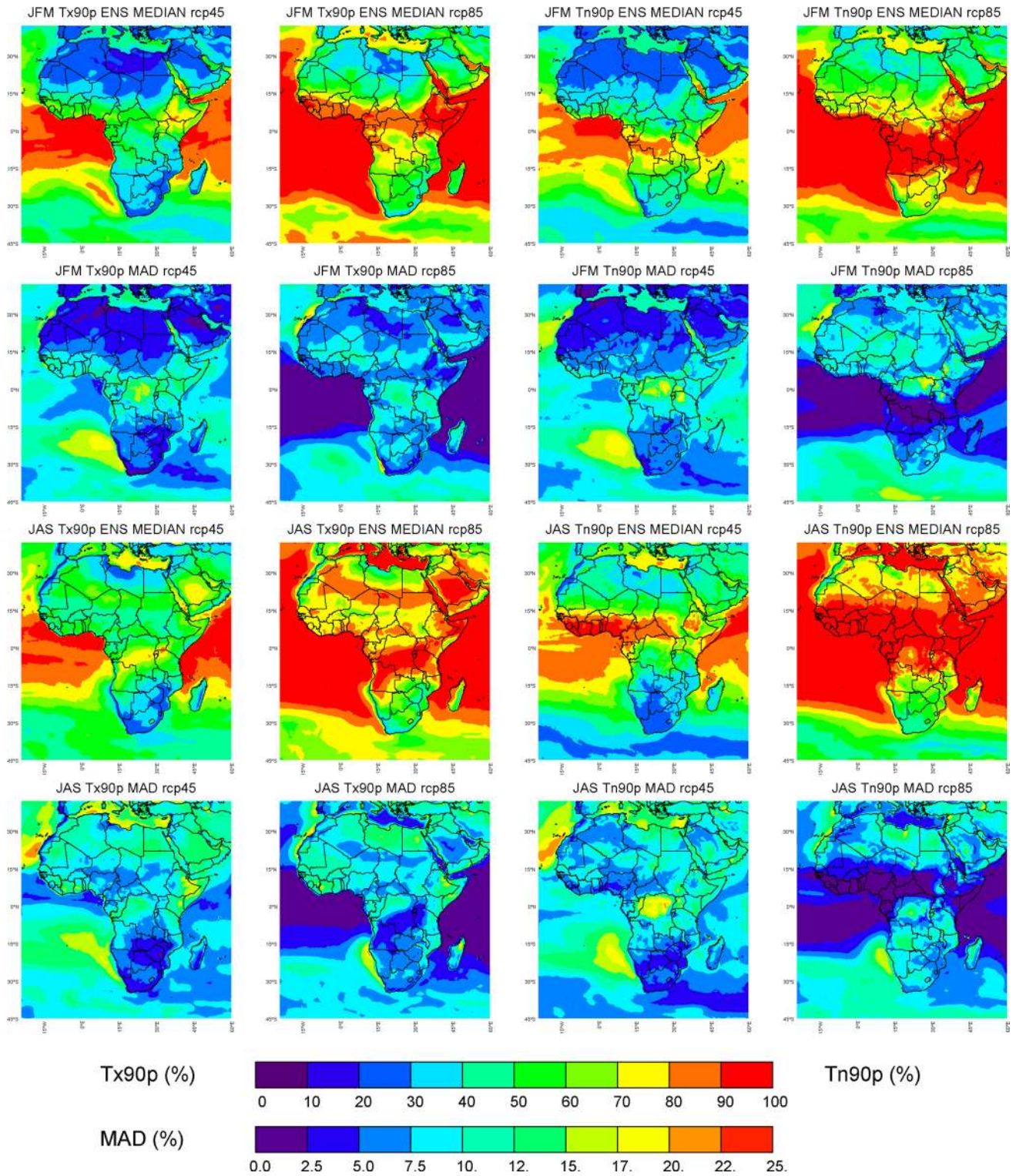

Fig. 8 Maps of projected Tx90p (warm days) and Tn90p (warm nights) indices at the end of the century (2071–2100) under RCP4.5 and RCP8.5, in JFM (*top two rows*) and JAS (*bottom two rows*). Results are shown as RCMs' ensemble median and inter-model variability (MAD)

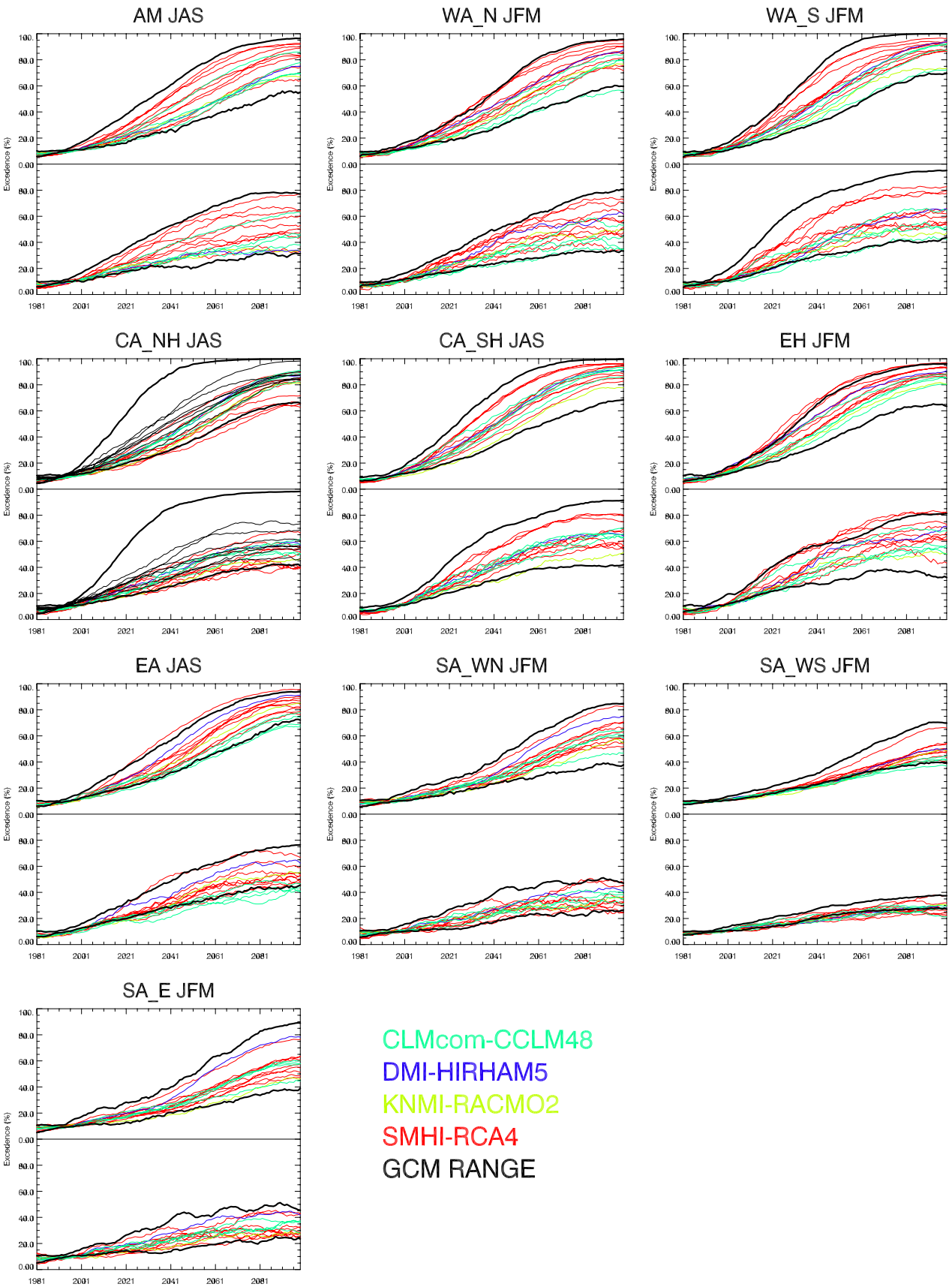

Fig. 9 As Fig. 3 for seasonal Tx90p (warm days). For CA_NH, all GCMs runs are also shown

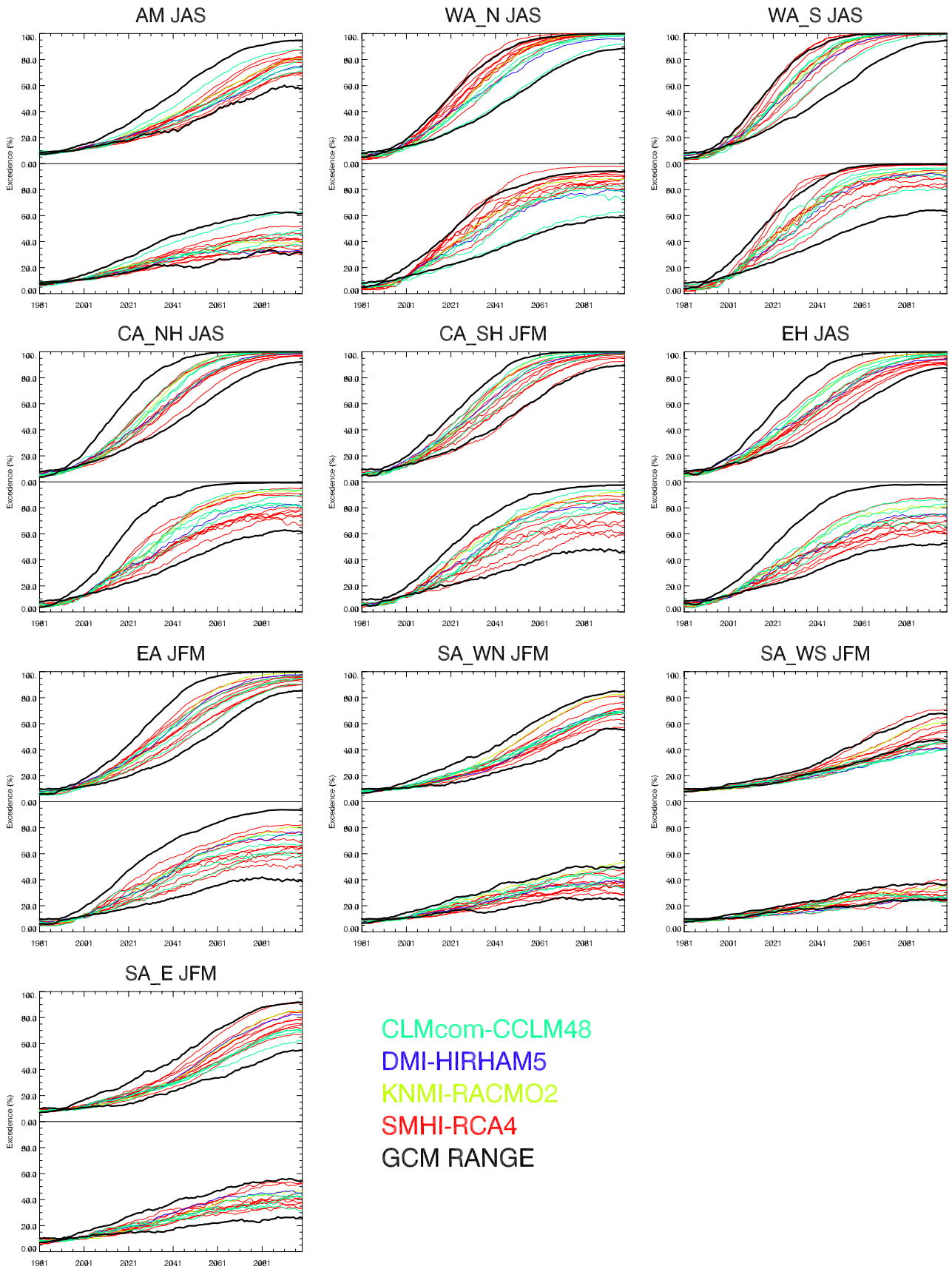

Fig. 10 As Fig. 3 but for seasonal Tn90p (warm nights)

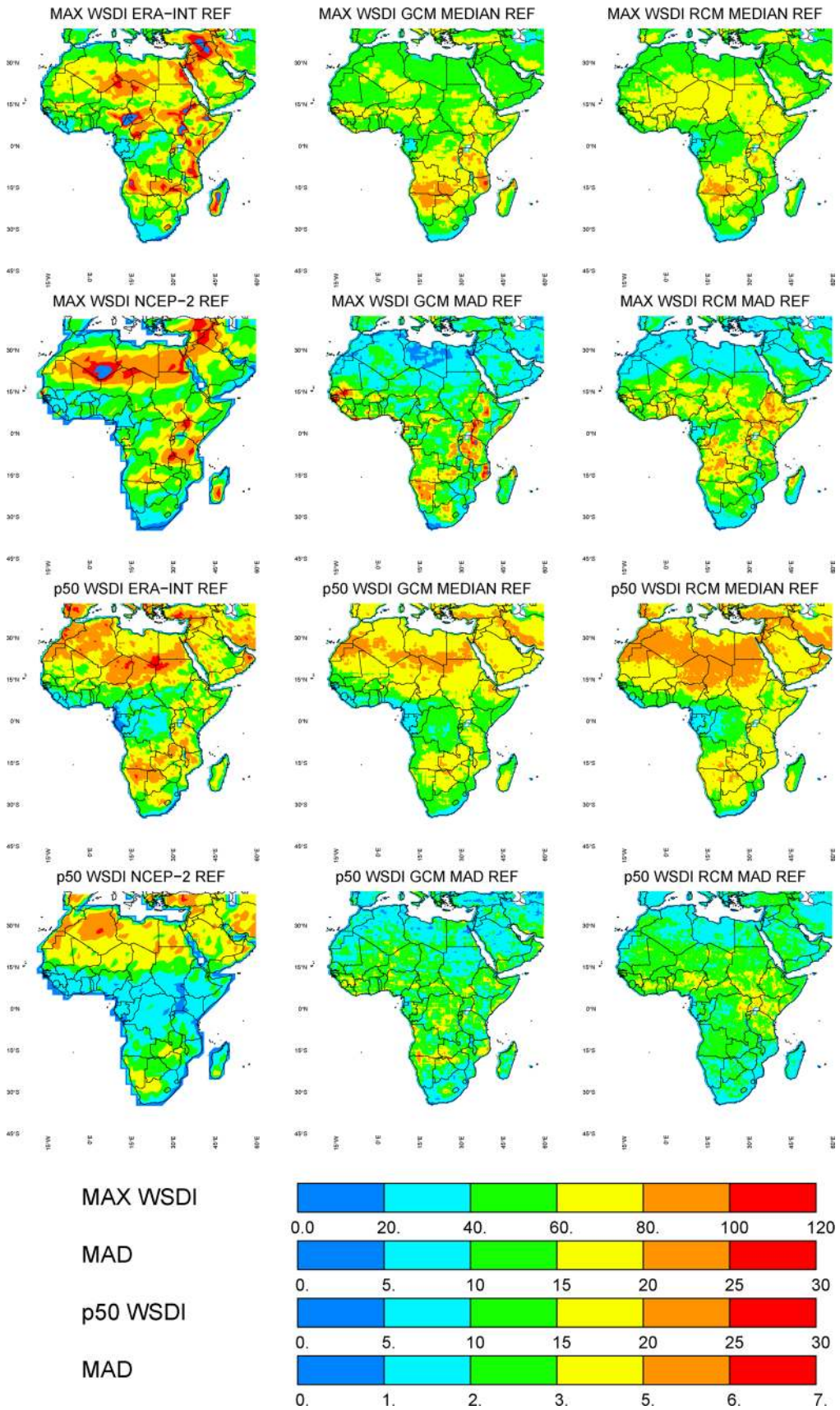
MAX WSDI ERA−INT REF
MAX WSDI GCM MEDIAN REF
MAX WSDI RCM MEDIAN REF
MAX WSDI NCEP−2 REF
MAX WSDI GCM MAD REF
MAX WSDI RCM MAD REF
p50 WSDI ERA−INT REF
p50 WSDI GCM MEDIAN REF
p50 WSDI RCM MEDIAN REF
p50 WSDI NCEP−2 REF
p50 WSDI GCM MAD REF
p50 WSDI RCM MAD REF
MAX WSDI
0.0 20. 40. 60. 80. 100 120
MAD
0. 5. 10 15 20 25 30
p50 WSDI
0. 5. 10 15 20 25 30
MAD
0. 1. 2. 3. 5. 6. 7.

◂**Fig. 11** Maps of Warm Spell Duration Index over the reference period (in days/year). Results are presented as temporal maximum (*first* and *second rows*) and median (p50, *third* and *fourth rows*) of WSDI annual values over the period 1981–2010. First column shows ERA-Interim and NCEP-2 results; GCMs and RCMs results are shown in the *second* and *third column*, respectively. Model results are shown as ensemble median ad MAD

climate change. For instance, Lustenberger et al. (2014) found a significant change in the upper and lower ends of the PDF of Tx and Tn over large areas of Europe, which results in an asymmetry between changes in the cold and warm extremes. Here we analyze two of the most significant examples, namely, CA_NH in JAS and SA_E in JFM.

Figure 6 shows, for each RCM, the PDF of daily Tx over CA_NH in JAS for the reference period (1981–2010) as well as at the end of the century (2071–2100) under RCP4.5 and RCP8.5, respectively. Here, PDFs are calculated simply as normalized frequency histograms of daily temperature values.

RCMs simulate present-day PDFs in a very heterogeneous way: for instance, CLMcom-CCLM48 and KNMI-RACMO2 reproduce the PDF calculated from ERA-Interim reanalysis rather satisfactorily, both for the mean and the standard deviation (which is a measure of the PDF width) close to those of ERA-Interim; DMI-HIRHAM5 reproduces the PDF width quite accurately, but sensibly overestimates its position (mean value); SMHI-RCA4 on the other hand misrepresents both the position and the width of the PDF for nearly all the GCM-driven runs, resulting in an overestimation of both the mean Tx value and its daily variability.

On the contrary, the future evolution of the Tx PDF is more influenced by the driving GCM: for instance all the four ICHEC-EARTH driven RCMs show only a slight increase in the PDF width, whereas both SMHI-RCA4 and CLMcom-CCLM48 project a larger increase in Tx variability when driven by MPI-ESM-LR. Also CLMcom-CCLM48 driven by CNRM-CM5, and SMHI-RCA4 driven by either MIROC5 or NorSME1 show a large increase in the PDF standard deviation. As shown by e.g. Schär et al. (2004) increase in variability in response to greenhouse-gas forcing would strongly affect the incidence of extreme events such as heat waves; this is true especially in tropical regions, where the present day variability is small, and it will be investigated later on.

In extra-tropic regions such as South Africa, present day observed daily Tx variability is larger, as shown in Fig. 7, with a value of the PDF standard deviation (2.6 °C) more than twice that of CA_NH (1.13 °C). RCMs tend in general to slightly underestimate mean Tx, especially all the runs driven by ICHEC-EARTH. The width of the PDF is usually too narrow, especially for DMI-HIRHAM5 and KNMI-RACMO2, whereas CLMcom-CCLM48 tends to simulate a larger daily variability, especially when driven by MPI-ESM-LR and CNRM-CM5. At the end of the century the PDF width has not changed significantly, especially for all SMHI-RCA4 runs and DMI-HIRHAM5, whereas CLMcom-CCLM48 (driven by ICHEC-EARTH and HadGEM2-ES) and KNMI-RACMO2 project a larger increase in variability. If the variability does not increase significantly, the frequency of extreme events is mostly related to the change of the mean Tx value.

Figure 8 shows the seasonal ensemble median and MAD of Tx90p (warm days) and Tn90p (warm nights) at the end of the century. As mentioned, these indices are defined as the percentage of days where Tx (Tn) is above the calendar day 90th percentile. As pointed out by Sillmann et al. (2013a), percentile based indices represent exceedance rates (in %) relative to the reference period (1981–2010), during which the average value of the index is 10 % by definition. The largest increase in Tx90p is found for both RCPs over sub equatorial Africa (Democratic Republic of Congo, Angola and Zambia), with values up to more than 90 % in JAS, whereas in JFM values of more than 80 % are found over the gulf of Guinea, Central African Republic, South Sudan and Ethiopia. Large variation in the seasonal Tx90p value are found over the Sahara, with JAS values nearly twice the JFM ones, whereas values over South Africa are more season independent, with an increase generally between 50 and 70 %.

Changes in Tn90p are usually larger than those of Tx90p, as already noted by e.g. Sillmann et al. (2013b); in particular, a large fraction of sub-equatorial Africa in JFM and the tropics in JAS show values of Tn90p larger than 90 %. In fact, in regions characterized by a small day to day variability (small values of the PDF standard deviation, see Fig. 6) relatively small changes in the mean temperature may produce large variations in the excendance values.

The temporal evolution of seasonal Tx90p is shown in Fig. 9 for selected areas. Large increase in the percentage of warm days is projected in all regions, although large differences exist amongst models. For instance, in WA_S in JFM SMHI-RCA4 driven by either CCma-CanESM2 or IPSL-CM5A projects Tx90p exceeding 80 % around 2050 (under RCP8.5), whereas CLMcom-CCLM48 driven by CNRM-CM5 projects an average exceedance of 67.2 % at the end of the century (2071–2100). Similarly, under RCP4.5 the largest Tx90p value (82.17 % for SMHI-RCA4 driven by IPSL-CM5A) is nearly twice the value of the smallest one (42.63 %, CLMcom-CCLM48 driven by CNRM-CM5). This contrasting behaviour can be further interpreted, for CA_NH in JAS and SA_E in JFM, by analyzing the PDF of Tx shown previously in Figs. 6 and 7, respectively. In SA_E two RCMs (DMI-HIRHAM5 and SMHI-RCA4 driven IPSL-CM5A) stand clearly out projecting the largest values of exceedance, being 73.07 and

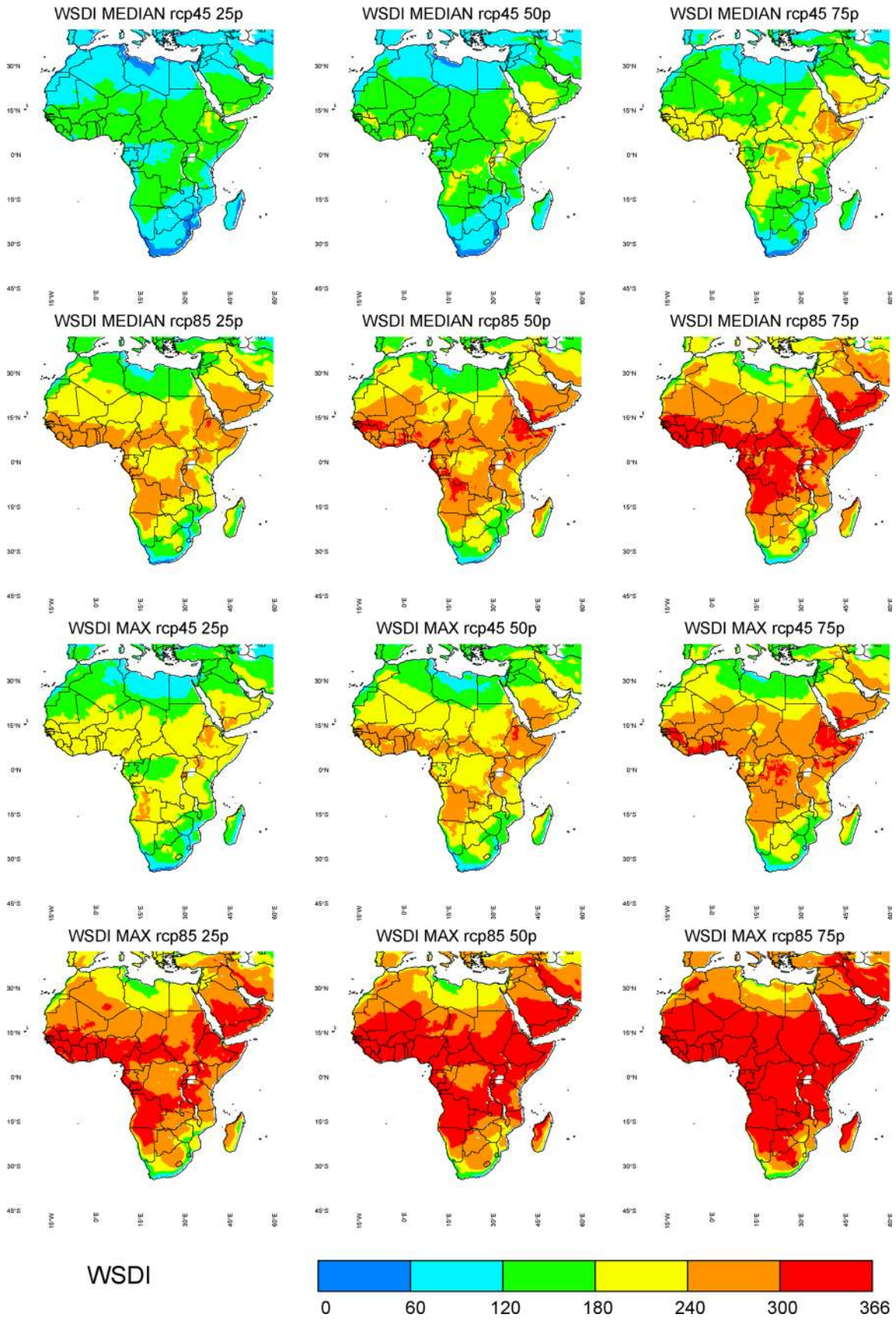
WSDI MEDIAN rcp45 25p
WSDI MEDIAN rcp45 50p
WSDI MEDIAN rcp45 75p
WSDI MEDIAN rcp85 25p
WSDI MEDIAN rcp85 50p
WSDI MEDIAN rcp85 75p
WSDI MAX rcp45 25p
WSDI MAX rcp45 50p
WSDI MAX rcp45 75p
WSDI MAX rcp85 25p
WSDI MAX rcp85 50p
WSDI MAX rcp85 75p
WSDI
0
60
120
180
240
300
366

◂**Fig. 12** Maps of Warm Spell Duration Index (in days/year) at the end of the century (2071–2100), under RCP4.5 and RCP8.5 as projected by the RCMs. Results are presented as temporal median (*first* and *second rows*) and maximum (*third* and *fourth rows*) of WSDI annual values over the period 2071–2100, thus corresponding to heat waves occurring every 2 and 30 years, respectively. The middle column shows the 50th percentile (median) of the RCMs' ensemble. Model uncertainty is shown as the 25th and 75th percentile (*left* and *right column*, respectively)

72.00 %, respectively, against the ensemble mean value of 53.83 %. The PDFs and their future evolution simulated by these models are however very different; SMHI-RCA4 simulates a PDF that is relatively wide (the standard deviation being 2.18 °C), similarly to the observed one, but it projects the largest increase in mean Tx, namely 5.8 °C. On the contrary, DMI-HIRHAM5 shows a smaller increase in mean Tx (3.9 °C) but, as the PDF is relatively narrow (the standard deviation being 1.69 °C), a large fraction of it exceeds the 90th historical percentile. The shape of the PDF is here crucial, as a similar or even higher increase of mean Tx (4.2 °C) on a PDF that is very wide produces only a 40.92 % value of exceedance at the end of the century. (CLMcom-CCLM48 driven by CNRM-CM5).

Similarly, for CA_NH in JAS, the smallest values of exceedance are associated with the smallest increase in mean Tx (between 3.0 °C and 3.4 °C), by SMHI-RCA4 driven by MIROC5, NCC-NorESM1 and CNRM-CM5. However, it is important to note that the historical PDF simulated by SMHI-RCA4 is largely wider than the ERA-Interim one. In cases where the PDF is narrower, similar increase in mean Tx (3.2 °C) leads to larger values of exceedance (78.19 % for KNMI-RACMO2), and to even larger values (85.75 %) when Tx increase reaches 4.4 °C (CLMcom-CCLM48 driven by ICHEC-EARTH).

Finally we note that the uncertainty in the RCMs' Tx90p projections is generally similar to the GCMs' one, with few notably exceptions, such as WA_S and CA_SH (under RCP4.5) and, especially, CA_NH. Here, in fact, three of the nine GCMs project an increase of TX90p larger than all RCMs, with IPSL-CM5A-MR standing clearly out projecting a value of exceedance larger than 80 % starting from 2035. It is difficult to infer the cause of this difference, as this GCM was downscaled only by SMHI-RCA4; given the large numerical domain used by the RCMs, it is however possible that over regions such as central Africa, away from the domain boundaries, local process and parameterizations (e.g. that for the soil) play a crucial role. For instance, Dosio and Panitz (2015) show that over central Africa the signal of projected precipitation for CLMcom-CCLM48 is the opposite of that of the driving GCMs.

Changes in the exceedance of warm nights (Tn90p) are mostly larger than those of Tx90p, as shown in Fig. 10. In particular, a large number of regions show values of Tn90p higher than 90 % at the end of the century, under RCP8.5 (WA_N, WA_S, CA_NH and EH in JAS, CA_SH, and EA in JFM), with some cases where all the RCMs project a nearly 100 % exceedance (99.54 % on ensemble average for WAS_S, and 97.90 % for CA_NH, in JAS). It is noteworthy that for the Gulf of Guinea (WA_S) and the Sahel (WA_N) in JAS, SMHI-RCA4 driven by HadGEM2-ES projects Tn90p reaching 95 % starting from around 2060 even under RCP4.5. Under this lower emission scenario, inter model variability is especially large, with values ranging for e.g., CA_SH in JFM, between 60.0 % (SMHI-RCA4 driven by CNRM-CM5) and 92.90 % (CLMcom-CCLM48 driven by HadGEM2-ES). The RCMs' uncertainty is generally as large as that of the driving GCMs, a part from WA_S, EH and EA (under RCP4.5) where it is reduced up to nearly 15 %.

3.3 Warm Spell Duration Index and Heat Waves Magnitude Index-daily

We first evaluate the ability of climate models to reproduce the main characteristics of heat waves over the reference period. Figure 11 shows the temporal maximum and median of WSDI annual values over the period 1981–2010. Large uncertainties exist between the WSDI maximum calculated from the reanalyses; for instance, over the Shara, NCEP-2 shows larger values than AER-Interim, whereas the contrary is true over the Horn of Africa, Cameroon, Nigeria, Central African republic ad Angola. Both GCMs and RCMs show generally similar results, usually underestimating WSDI maximum over the Sahara (although RCMs results compare better to the reanalysis). Local differences are visible also e.g. over northern Mozambique, where GCMs overestimate WSDI maximum and RCMs underestimate it.

ERA-Interim shows values of median WSDI larger than NCEP-2, a part from Central Africa.GCMs and RCMs results are generally similar and closer to ERA-Interim than NCEP-2; regional models perform slightly better locally over Niger, Chad, Somalia, Namibia and south Africa. Finally, inter-model variability is very similar between GCMs and RCMs.

Figure 12 shows maps of WSDI as modelled by RCMs at the end of the century. Here, the median and maximum of the yearly WSDI can be regarded as WSDI values projected to occur every two and 30 years, respectively.

The RCMs' ensemble median shows a large fraction of Africa facing, once every 2 years, heat waves with WSDI values longer than four (under RCP4.5) and six months (under RCP8.5). Under the most severe emission scenario, some models (75-th percentile of the RCM ensemble) project that the gulf of Guinea, Central Africa and the Horn of

Table 3 Climate change signal (under RCP8.5) of seasonal mean temperature for AM in JFM (averaged over land points only)

GCM /RCM	CLMcom-CCLM48	DMI-HIRHAM5	KNMI-RACMO2	SMHI-RCA4	Mean	δ
ICHEC-EC-EARTH	2.86	3.05	3.87	3.51	3.32	1.01
MOHC-HadGEM2-ES	4.28			5.08	4.68	0.80
CNRM-CERFACS-CNRM-CM5	2.45			3.23	2.84	0.78
MPI-M-MPI-ESM-LR	2.97			3.91	3.44	0.94
CCma-CanESM2				4.19	4.19	
MIROC-MIRCO5				4.86	4.86	
NCC-NorESM1-M				3.25	3.25	
IPSL-IPSL-CM5A-MR				4.95	4.95	
NOAA-GFDL-GFDL-ESM2M				3.19	3.19	
Mean	3.14	3.05	2.87	4.02 (3.93)	**3.71**	
δ	1.84			1.90 (1.86)		**2.63**

All GCM-RCM runs are grouped according to the downscaling RCM (column) and driving GCM (row); for each group also reported are the average and the intra-model spread (δ, i.e. maximum–minimum). For SMHI-RCA4 the values of the mean and spread of the runs driven by the same 4 GCMs as CLMcom-CLM48 are reported in bracket. Bold values are the entire ensemble mean and spread. Units are in degrees Celsius

Table 4 As 3 for CA_SH in JAS

GCM RCM	CLMcom-CCLM48	DMI-HIRHAM5	KNMI-RACMO2	SMHI-RCA4	Mean	δ
ICHEC-EC-EARTH	4.14	3.58	3.66	4.42	3.95	0.83
MOHC-HadGEM2-ES	5.25			5.15	5.20	0.11
CNRM-CERFACS-CNRM-CM5	3.81			3.57	3.69	0.23
MPI-M-MPI-ESM-LR	5.62			5.00	5.31	0.62
CCma-CanESM2				4.90	4.90	
MIROC-MIRCO5				4.40	4.40	
NCC-NorESM1-M				3.66	3.66	
IPSL-IPSL-CM5A-MR				5.51	5.51	
NOAA-GFDL-GFDL-ESM2M				4.07	4.07	
Mean	4.70	3.58	3.66	4.52 (4.54)	**4.45**	
δ	1.81			1.94 (1.57)		**2.04**

Bold values are the entire ensemble mean and spread

Table 5 As 3 for SA_E in JAS

GCM RCM	CLMcom-CCLM48	DMI-HIRHAM5	KNMI-RACMO2	SMHI-RCA4	Mean	δ
ICHEC-EC-EARTH	5.42	4.35	3.69	3.72	4.30	1.73
MOHC-HadGEM2-ES	5.31			4.44	4.88	0.87
CNRM-CERFACS-CNRM-CM5	4.30			3.53	3.91	0.76
MPI-M-MPI-ESM-LR	5.64			4.38	5.01	1.25
CCma-CanESM2				4.57	4.57	
MIROC-MIRCO5				3.66	3.66	
NCC-NorESM1-M				2.97	2.97	
IPSL-IPSL-CM5A-MR				5.98	5.98	
NOAA-GFDL-GFDL-ESM2M				3.19	3.19	
Mean	5.17	4.35	3.69	4.05 (4.02)	**4.34**	
δ	1.34			3.01 (0.91)		**3.01**

Bold values are the entire ensemble mean and spread

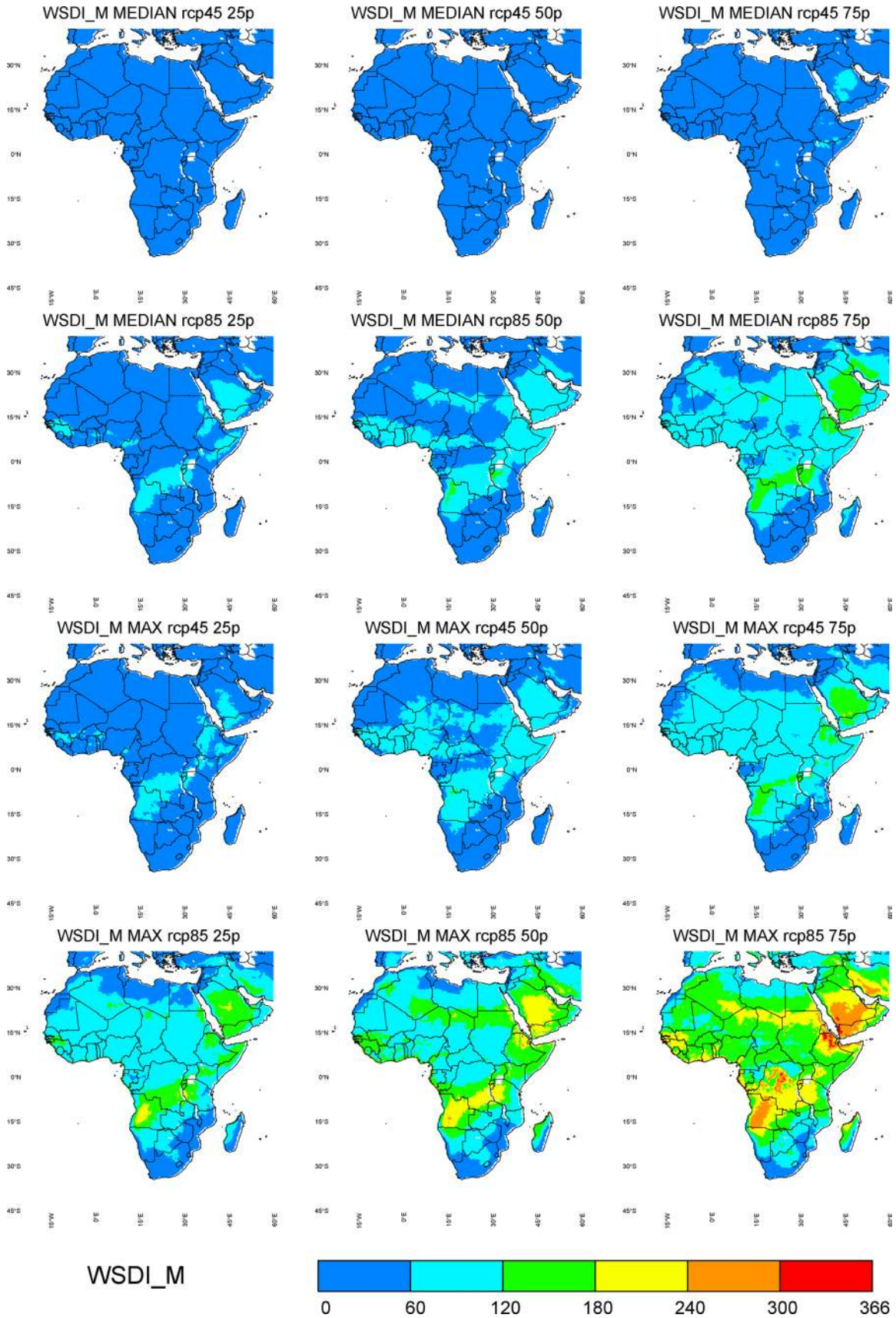

Fig. 13 As Fig. 12 but for the maximum annual value of the Warm Spell Duration Index (HWMI_M)

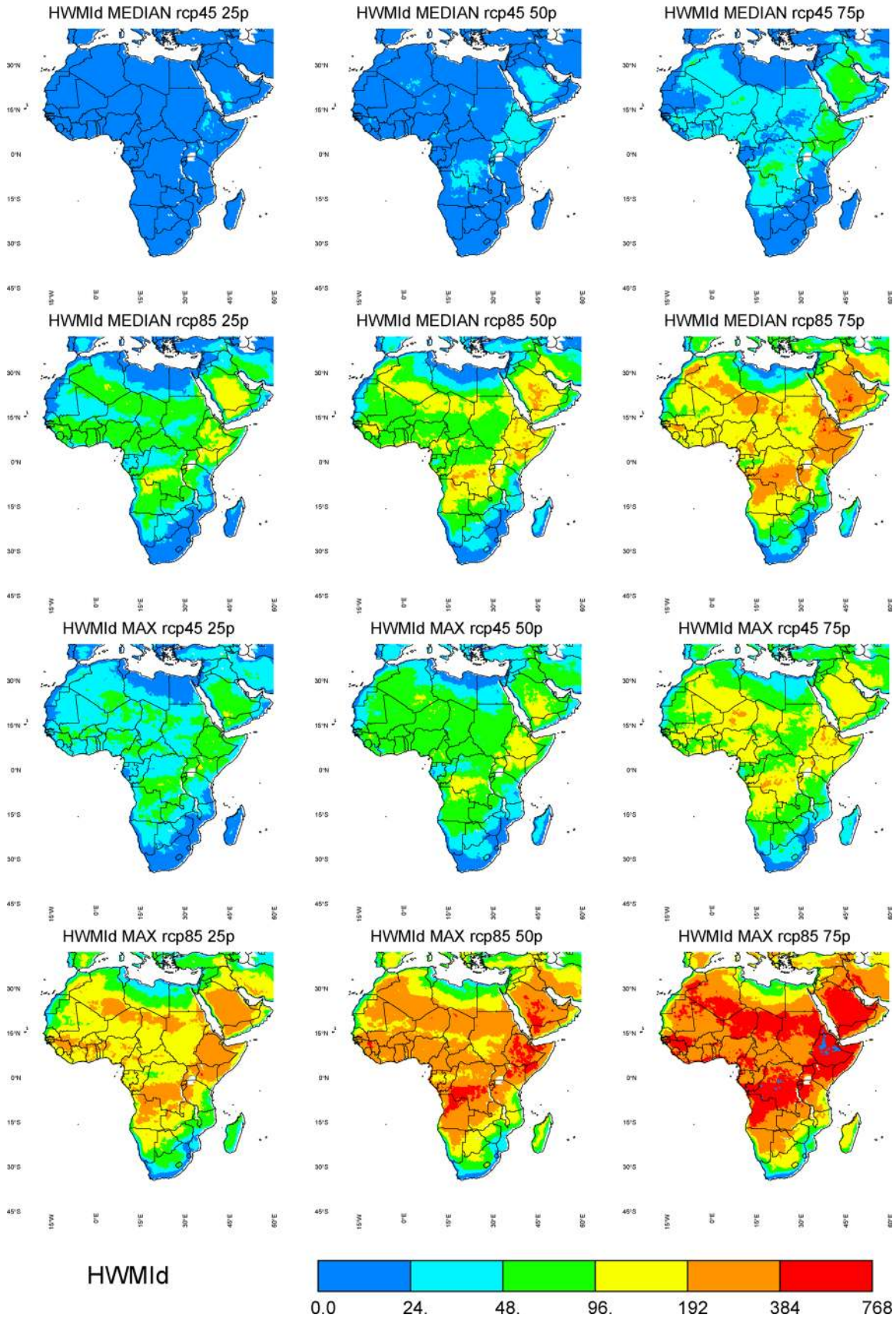

Fig. 14 As Fig. 12 but for the Heat Wave Magnitude Index daily

Africa will be affected, once every 2 years, by warm spells with a total length of more than 300 days.

It is interesting to note, that WSDI maximum under RCP4.5 is generally lower than the WSDI median under RCP8.5, meaning that under the most extreme emission scenario, the total length of heat spells that will occur normally (i.e. once every 2 years) will be longer than those occurring once every 30 years under the lower emission scenario.

In order to analyze more thoroughly the characteristics of the heat waves, Fig. 13 shows, similarly to Fig. 12, the temporal median and maxima of the length of the single longest warm spell (indicated as WSDI_M). The RCM's ensemble median shows that under RCP8.5 the gulf of Guinea, the Horn of Africa, the Arabian peninsula, Angola and the Democratic Republic of Congo are projected to face, every 2 years, heat waves of length between 60 and 120 days. Once every 30 years heat waves are projected to be longer than 180 days over part of central Africa and the Arabian peninsula.

It is interesting to note that over the gulf of Guinea the WSDI_M median and maxima under RCP8.5 have similar values (whereas for instance over Angola and the Arabian peninsula WSDI_M maximum is twice the median value). This means that this region will not be affected by extremely long heat waves, but they may be relatively frequent, causing the WSDI value to reach, once every 30 years, very high values (more than 300, see Fig. 12).

As explained, WSDI (or WSDI_M) is a measure of the length of the warm spell, but it does not take into account its intensity; as a result, two warm spells of the same length but with different values of Tx, will have the same value of WSDI (Russo et al. 2014).

On the contrary, HWMId is designed to take into account both the length and intensity of the heat wave, and, in addition, its value is weighted with respect to the climatological maximum temperature interquantile range. Results for HWMId are shown in Fig. 14. By comparing the results for HWMId and WSDI, some similarities can be noted, along with some striking differences. In particular, we first note

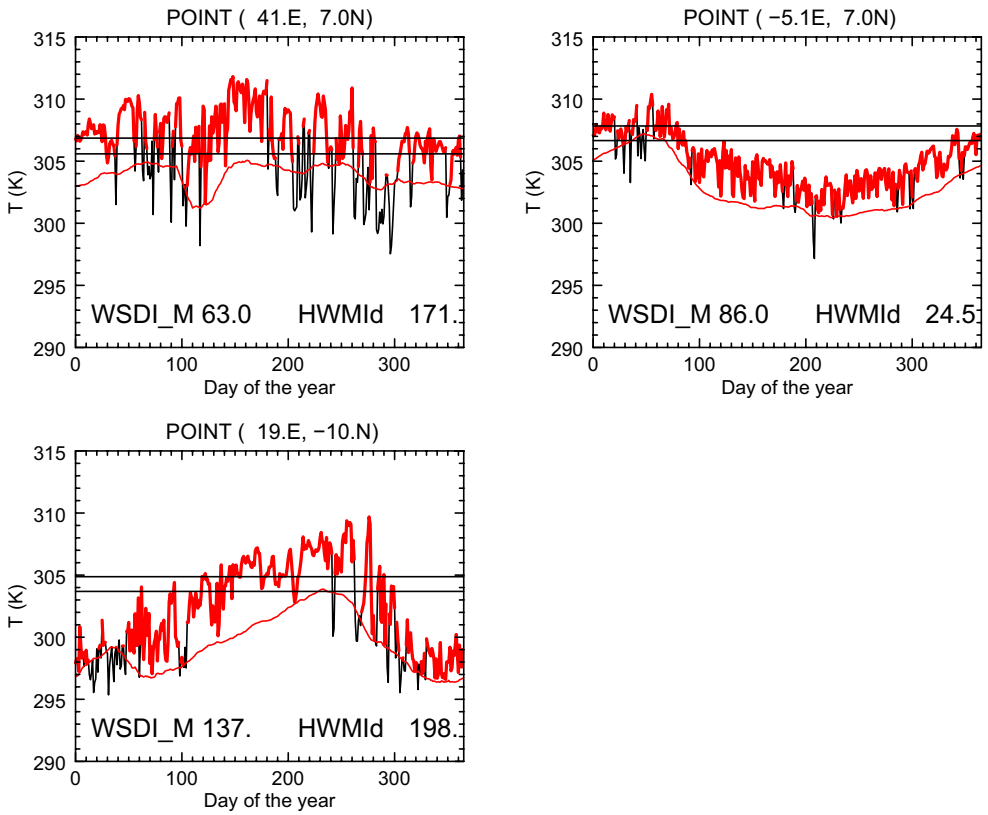

Fig. 15 Time evolution of Tx, for one RCM (KNMI-RACMO2), in 2098 under RCP8.5 for a single grid point in the Horn of Africa (41°E, 7°N), the gulf of Guinea (−5.1°E, 7°N) and central Africa (19°E, −10°N). The calendar 90-th percentile of Tx in the reference period is also shown (*thin red line*): by definition, a heat wave occurs when Tx is above the 90-th percentile for at least 3 consecutive days (shown as *thick red line*). Also shown in the picture are T_{30y25p} and T_{30y75p} ,i.e., the 25-th and 75-th percentiles of the yearly maximum temperatures over the reference period (*horizontal black lines*). By definition, only the days when daily maximum temperature is higher than T_{30y25p} contribute to the value of HWMId (see Eq. 1)

that, at the end of the century, HWMId reaches the highest values, in median, over central Africa, the Horn of Africa, and the Arabian peninsula, under either RCP. This is consistent with the results of WSDI (and WSDI_M) over these regions affected by very long heat spells. We also note that, similarly to WSDI, the median value of HWMId under RCP8.5 is larger than the maximum value under RCP4.5, meaning that under the most severe emission scenario heat waves may be not only longer, but also more intense.

The largest discrepancy between WSDI and HWMId maps is shown over the gulf of Guinea where, in median, HWMId has a relatively smaller value, compared to e.g. the horn of Africa, despite the fact that both WSDI and WSDI_M have similar values over these two regions, i.e. the length of the heat waves are comparable, but intensities differ.

It is important to understand that WSDI (WSDI_M) and HWMId give different but complementary information on the nature of heat waves; in particular the value of HWMId it is indeed proportional to the heat wave length, but it also depends, crucially, on the temperature anomaly with respect the climatological 25-th percentile, as explained. As a result, it is possible that relatively short but intense heat waves (i.e. with very high values of Tx) may have values of HWMId larger than long but 'weak' warm spells. In order to better investigate the origin of the difference between the two indices, Fig. 15 shows, as an example, the yearly evolution of Tx, for one RCM, in 2098 (under RCP8.5) for a single grid point in the Horn of Africa (41°E, 7°N), the gulf of Guinea (-5.1°E, 7°N) and central Africa (19°E, −10°N). The calendar 90-th percentile of Tx in the reference period is also shown: by definition, a heat wave occurs when Tx is above the 90-th percentile for at least 3 consecutive days (shown as thick red line). In addition, only the days when daily maximum temperature is higher than T_{30y25p} contribute to the value of HWMId (see Eq. 1); from Fig. 15 we note that over the Horn of Africa, the relatively 'short' heat wave occurring in April and May (WSDI_M = 63) produces a very high value of HWMId (HWMId = 171) due to the large Tx anomaly with respect to T_{30y75p}. On the contrary, over the gulf of Guinea, the longest heat wave (WSDI_M = 86) does not contribute to HWMId, whose relatively small value (HWMId = 24.5) is due to the short heat wave occurring in March. Finally, over central Africa, HWMId reaches very high values due to a combination of very long and intense heat waves.

4 Summary and concluding remarks

In this work we have analyzed the projections of temperature and related extreme events for Africa based on the results of a large ensemble of CORDEX RCMs. In particular, we have investigated not only the seasonal climatology of mean, minimum and maximum temperature, but also percentile based indices of extreme events, namely Tx90p and Tn90p, and we have related them to the temperature probability distribution function, both in the present and future climate. Finally, projections of heat waves occurrences were analyzed by means of two different indices, the widely used Warm Spell Duration Index, which takes into account only the length of a warm spell, and a recently developed Heat Wave Magnitude Index-daily that takes into account also its intensity.

Future projections under the RCP4.5 scenario show a general increase of mean temperature of around 2 °C over the whole continent in JFM, whereas in JAS warming up to 3 °C is found over north-equatorial Africa and the Arabian peninsula. Under the more severe RCP8.5 scenario warming in JFM reaches 5 °C over South Africa, Chad, Central African Republic and South Sudan, whereas in JAS temperatures over large part of Northern Africa, the Sahara and the Arabian peninsula are projected to increase up to 6 °C. However, model results can differ greatly, with values of the median absolute deviation reaching 1.6 °C.

RCMs simulate present climate temperature PDF heterogeneously; depending on the season and region, some RCMs show a PDF similar to that calculated with ERA-Interim, whereas other misrepresent its position or width, and, in some cases, both. However, the future evolution of the PDF is also strongly influenced by the driving GCM.

Concerning extreme events indices, the largest increase in the number of warm days (Tx90p) is found for both RCPs over sub equatorial Africa, with exceedance rates projected to reach up to more than 90 % in JAS, and more than 80 % in JFM over the gulf of Guinea, Central African Republic, South Sudan and Ethiopia. Values over South Africa are more season independent, with an increase generally between 50 and 70 %.

Changes in the number of warm nights (Tn90p) are usually larger than those of Tx90p; in particular, a large fraction of sub-equatorial Africa in JFM and the tropics in JAS show, at the end of the century, values of Tn90p larger than 90 %. In fact, in regions characterized by a small day to day variability relatively small changes in the mean temperature may produce large variations in the excendance values. It is noteworthy that for the Gulf of Guinea and the Sahel in JAS, SMHI-RCA4 driven by HadGEM2-ES projects Tn90p reaching 95 % starting from around 2060 even under RCP4.5, although under this lower emission scenario, inter model variability is especially large.

The impact of an heat wave is related not only to its length (and frequency), but also to its intensity. RCM's results show that under RCP8.5 the gulf of Guinea, the Horn of Africa, the Arabian peninsula, Angola and the Democratic Republic of Congo are expected to face, every

2 years, heat waves of length between 60 and 120 days. Once every 30 years heat waves are projected to be longer than 180 days over part of central Africa and the Arabian peninsula. In addition, it was shown that the total length of heat spells projected to occur normally (i.e. once every 2 years) under RCP8.5 may be longer than those occurring once every 30 years under the lower emission scenario.

By employing the recently developed HWMId index, it was possible to investigate the relationship between heat wave length ad intensity; in particular it was shown that very intense heat waves such as that occurring over the Horn of Africa may have values of HWMId larger than that of even longer, but relatively weak, heat waves over West Africa; as such WSDI and HWMI give different but complementary information on the nature of heat waves.

Finally, it is worth remembering that although this work is based on a relatively large ensemble of RCMs' results, the GCM-RCM matrix is far from being complete, with only one RCM downscaling a large number of GCMs (8). As it was shown that results may depend strongly on the RCM, subsequently, the uncertainty on the results due to inter-model variability may increase if more runs were added to the matrix. This would be essential in order to identify and quantify the many sources of uncertainty that still remain.

Acknowledgments We acknowledge the World Climate Research Programme's Working Group on Coupled Modelling, which is responsible for CMIP, and all the modelling groups that performed the simulations and made their data available. CORDEX-Africa results are openly available through the Earth System Grid Federation (ESGF) server. NCEP Reanalysis 2 data is provided by the NOAA/OAR/ESRL PSD, Boulder, Colorado, USA, from their Web site at http://www.esrl.noaa.gov/psd/ Hans-Juergen Panitz (KIT) is acknowledged for producing Fig. 1. Discussions with Simone Russo (JRC) have been very useful and greatly appreciated.

References

Alexander LV, Zhang X, Peterson TC, Caesar J, Gleason B, Klein Tank aMG, Haylock M, Collins D, Trewin B, Rahimzadeh F, Tagipour A, Rupa Kumar K, Revadekar J, Griffiths G, Vincent L, Stephenson DB, Burn J, Aguilar E, Brunet M, Taylor M, New M, Zhai P, Rusticucci M, Vazquez-Aguirre JL (2006) Global observed changes in daily climate extremes of temperature and precipitation. J Geophys Res 111(D5):D05,109. doi:10.1029/2005JD006290

Brands S, Herrera S, Fernández J, Gutiérrez JM (2013) How well do CMIP5 earth system models simulate present climate conditions in Europe and Africa? Clim Dyn 41(3–4):803–817. doi:10.1007/s00382-013-1742-8

Buontempo C, Mathison C, Jones R, Williams K, Wang C, McSweeney C (2014) An ensemble climate projection for Africa. Clim Dyn. doi:10.1007/s00382-014-2286-2

Coppola E, Giorgi F, Raffaele F, Fuentes-Franco R, Giuliani G, LLopart-Pereira M, Mamgain A, Mariotti L, Diro GT, Torma C (2014) Present and future climatologies in the phase I CREMA experiment. Clim Change pp 23–38. doi:10.1007/s10584-014-1137-9

Crétat J, Vizy EK, Cook KH (2013) How well are daily intense rainfall events captured by current climate models over Africa? Clim Dyn. doi:10.1007/s00382-013-1796-7

Dee D et al (2011) The ERAInterim reanalysis: configuration and performance of the data assimilation system. Q J R Meteorol Soc 137:553–597

Diaconescu EP, Laprise R (2013) Can added value be expected in RCM-simulated large scales? Clim Dyn 41(7–8):1769–1800. doi:10.1007/s00382-012-1649-9

Diallo I, Sylla MB, Giorgi F, Gaye aT, Camara M (2012) Multimodel GCM-RCM ensemble-based projections of temperature and precipitation over West Africa for the early 21st century. Int J Geophys 2012:1–19. doi:10.1155/2012/972896

Diallo I, Giorgi F, Deme A, Tall M, Mariotti L, Gaye AT (2016) Projected changes of summer monsoon extremes and hydroclimatic regimes over West Africa for the twenty-first century. Clim Dyn pp 1–24

Donat MG, Alexander LV, Yang H, Durre I, Vose R, Dunn RJH, Willett KM, Aguilar E, Brunet M, Caesar J, Hewitson B, Jack C, Klein Tank aMG, Kruger aC, Marengo J, Peterson TC, Renom M, Oria Rojas C, Rusticucci M, Salinger J, Elrayah aS, Sekele SS, Srivastava aK, Trewin B, Villarroel C, Vincent La, Zhai P, Zhang X, Kitching S (2013) Updated analyses of temperature and precipitation extreme indices since the beginning of the twentieth century: The HadEX2 dataset. J Geophys Res Atmos 118:2098–2118. doi:10.1002/jgrd.50150

Donat MG, Sillmann J, Wild S, Alexander LV, Lippmann T, Zwiers FW (2014) Consistency of temperature and precipitation extremes across various global gridded in situ and reanalysis datasets*. J Clim 27(13):5019–5035. doi:10.1175/JCLI-D-13-00405.1

Dosio A, Panitz HJ (2015) Climate change projections for CORDEX-Africa with COSMO-CLM regional climate model and differences with the driving global climate models. Clim Dyn. doi:10.1007/s00382-015-2664-4

Dosio A, Panitz HJ, Schubert-Frisius M, Lüthi D (2015) Dynamical downscaling of CMIP5 global circulation models over CORDEX-Africa with COSMO-CLM: evaluation over the present climate and analysis of the added value. Clim Dyn 44(9–10):2637–2661. doi:10.1007/s00382-014-2262-x

Endris HS, Omondi P, Jain S, Lennard C, Hewitson B, Chang'a L, Awange JL, Dosio A, Ketiem P, Nikulin G, Panitz HJ, Büchner M, Stordal F, Tazalika L (2013) Assessment of the performance of CORDEX regional climate models in simulating east African rainfall. J Clim 26(21):8453–8475. doi:10.1175/JCLI-D-12-00708.1

Fontaine B, Janicot S, Monerie PA (2013) Recent changes in air temperature, heat waves occurrences, and atmospheric circulation in Northern Africa. J Geophys Res Atmos 118:8536–8552. doi:10.1002/jgrd.50667

Gbobaniyi E, Sarr A, Sylla MB, Diallo I, Lennard C, Dosio A, Dhiédiou A, Kamga A, Klutse NAB, Hewitson B, Nikulin G, Lamptey B (2014) Climatology, annual cycle and interannual variability of precipitation and temperature in CORDEX simulations over West Africa. Int J Climatol 34(7):2241–2257. doi:10.1002/joc.3834

Giorgi F, Jones C, Asrar G (2009) Addressing climate information needs at the regional level: the CORDEX framework. Organization (WMO). Bulletin 58:175–183

Giorgi F, Coppola E, Raffaele F, Diro GT, Fuentes-Franco R, Giuliani G, Mamgain A, Llopart MP, Mariotti L, Torma C (2014) Changes in extremes and hydroclimatic regimes in the CREMA ensemble projections. Clim Change pp 39–51. doi:10.1007/s10584-014-1117-0

Haensler A, Saeed F, Jacob D (2013) Assessing the robustness of projected precipitation changes over central Africa on the basis of a multitude of global and regional climate projections. Clim Change 121(2):349–363. doi:10.1007/s10584-013-0863-8

IPCC (2007) Climate change 2007: the physical science basis: contribution of Working Group I to the Fourth Assessment Report of the Intergovernmental Panel on Climate Change. Cambridge University Press, Cambridge

IPCC (2012) Managing the risks of extreme events and disasters to advance climate change adaptation. Research Report pp 1–594, doi:10.1017/CBO9781139177245

James R, Washington R, Rowell DP (2013) Implications of global warming for the climate of African rainforests. Phil Trans R Soc Lond B. doi:10.1098/rstb.2012.0298

Justino F, Stordal F, Clement A, Coppola E, Setzer A, Brumatti D (2013) Modelling weather and climate related fire risk in Africa. Am J Clim Change 2:209–224. doi:10.4236/ajcc.2013.24022

Kalognomou EA, Lennard C, Shongwe M, Pinto I, Favre A, Kent M, Hewitson B, Dosio A, Nikulin G, Panitz HJ, Büchner M (2013) A diagnostic evaluation of precipitation in CORDEX models over Southern Africa. J Clim 26(23):9477–9506. doi:10.1175/JCLI-D-12-00703.1

Kanamitsu M, Ebisuzaki W, Woollen J, Yang SK, Hnilo JJ, Fiorino M, Potter GL (2002) NCEPDOE AMIP-II Reanalysis (R-2). Bull Am Meteorol Soc 83(11):1631–1643. doi:10.1175/BAMS-83-11-1631

Kim J, Kim T, Arritt R, Miller N (2002) Impacts of increased atmospheric CO2 on the hydroclimate of the Western United States. J Clim 15:1926–1942

Kim J, Waliser DE, Ca Mattmann, Goodale CE, Hart AF, Pa Zimdars, Crichton DJ, Jones C, Nikulin G, Hewitson B, Jack C, Lennard C, Favre A (2014) Evaluation of the CORDEX-Africa multi-RCM hindcast: systematic model errors. Clim Dyn 42(5–6):1189–1202. doi:10.1007/s00382-013-1751-7

Krähenmann S, Kothe S, Panitz HJ, Ahrens B (2013) Evaluation of daily maximum and minimum 2-m temperatures as simulated with the Regional Climate Model COSMO-CLM over Africa. Meteorol Z 22(3):297–316. doi:10.1127/0941-2948/2013/0468

Laprise R, Hernández-Díaz L, Tete K, Sushama L, Šeparović L, Martynov A, Winger K, Valin M (2013) Climate projections over CORDEX Africa domain using the fifth-generation Canadian Regional Climate Model (CRCM5). Clim Dyn. doi:10.1007/s00382-012-1651-2

Lee JW, Hong SY (2013) Potential for added value to downscaled climate extremes over Korea by increased resolution of a regional climate model. Theor Appl Climatol. doi:10.1007/s00704-013-1034-6

Lee JW, Hong SY, Chang EC, Suh MS, Kang HS (2013) Assessment of future climate change over East Asia due to the RCP scenarios downscaled by GRIMs-RMP. Clim Dyn 42(3–4):733–747. doi:10.1007/s00382-013-1841-6

Lustenberger A, Knutti R, Fischer EM (2014) Sensitivity of European extreme daily temperature return levels to projected changes in mean and variance. J Geophys Res Atmos 119(6):3032–3044. doi:10.1002/2012JD019347

Lyon B (2009) Southern Africa summer drought and heat waves: observations and coupled model behavior. J Clim 22:6033–6046. doi:10.1175/2009JCLI3101.1

Mariotti L, Diallo I, Coppola E, Giorgi F (2014) Seasonal and intraseasonal changes of African monsoon climates in 21st century CORDEX projections. Clim Change, pp 1–13. doi:10.1007/s10584-014-1097-0

Moss RH, Ja Edmonds, Ka Hibbard, Manning MR, Rose SK, van Vuuren DP, Carter TR, Emori S, Kainuma M, Kram T, Ga Meehl, Mitchell JFB, Nakicenovic N, Riahi K, Smith SJ, Stouffer RJ, Thomson AM, Weyant JP, Wilbanks TJ (2010) The next generation of scenarios for climate change research and assessment. Nature 463(7282):747–56. doi:10.1038/nature08823

Nandozi CS, Omondi P, Komutunga E, Aribo L, Isubikalu P, Tenywa MM (2012) Regional climate model performance and prediction of seasonal rainfall and surface temperature of uganda. Afr Crop Sci J 20(s2):213–225

New M, Hewitson B, Stephenson DB, Tsiga A, Kruger A, Manhique A, Gomez B, Coelho CaS, Masisi DN, Kululanga E, Mbambalala E, Adesina F, Saleh H, Kanyanga J, Adosi J, Bulane L, Fortunata L, Mdoka ML, Lajoie R (2006) Evidence of trends in daily climate extremes over southern and west Africa. J Geophys Res 111(D14):D14,102. doi:10.1029/2005JD006289

Nikulin G, Jones C, Giorgi F, Asrar G, Büchner M, Cerezo-Mota R, Christensen OB, Déqué M, Fernandez J, Hänsler A, van Meijgaard E, Samuelsson P, Sylla MB, Sushama L (2012) Precipitation climatology in an ensemble of CORDEX-Africa regional climate simulations. J Clim 25(18):6057–6078. doi:10.1175/JCLI-D-11-00375.1

Orlowsky B, Seneviratne SI (2011) Global changes in extreme events: regional and seasonal dimension. Clim Change 110(3–4):669–696. doi:10.1007/s10584-011-0122-9

Paeth H, Mannig B (2012) On the added value of regional climate modeling in climate change assessment. Clim Dyn 41(3–4):1057–1066. doi:10.1007/s00382-012-1517-7

Perkins SE (2011) Biases and model agreement in projections of climate extremes over the tropical Pacific. Earth Interactions 15(24):1–36. doi:10.1175/2011EI395.1

Perkins SE, Alexander LV (2013) On the measurement of heat waves. J Clim 26(13):4500–4517. doi:10.1175/JCLI-D-12-00383.1

Perkins SE, Alexander LV, Nairn JR (2012) Increasing frequency, intensity and duration of observed global heatwaves and warm spells. Geophys Res Lett 39:1–5. doi:10.1029/2012GL053361

Pinto I, Lennard C, Tadross M, Hewitson B, Dosio A, Nikulin G, Panitz HJ, Shongwe ME (2015) Evaluation and projections of extreme precipitation over southern Africa from two CORDEX models. Clim Change. doi:10.1007/s10584-015-1573-1

Radinović D, Ćurić M (2012) Criteria for heat and cold wave duration indexes. Theoret Appl Climatol 107:505–510. doi:10.1007/s00704-011-0495-8

Russo S, Sterl A (2011) Global changes in indices describing moderate temperature extremes from the daily output of a climate model. J Geophys Res 116(D3):D03,104. doi:10.1029/2010JD014727

Russo S, Dosio A, Graversen RG, Sillmann J, Carrao H, Dunbar MB, Singleton A, Montagna P, Barbola P, Vogt JV (2014) Magnitude of extreme heat waves in present climate and their projection in a warming world. J Geophys Res Atmos 119(22):12500–12512. doi:10.1002/2014JD022098

Russo S, Sillmann J, Fischer EM (2015) Top ten European heatwaves since 1950 and their occurrence in the coming decades. Environ Res Lett 10(12):124003. doi:10.1088/1748-9326/10/12/124003

Schär C, Vidale PL, Lüthi D, Frei C, Häberli C, Ma Liniger, Appenzeller C (2004) The role of increasing temperature variability in European summer heatwaves. Nature 427:332–336. doi:10.1038/nature02300

Sillmann J, Kharin VV, Zhang X, Zwiers FW, Bronaugh D (2013a) Climate extremes indices in the CMIP5 multimodel ensemble: part 1. Model evaluation in the present climate. J Geophys Res Atmos 118(4):1716–1733. doi:10.1002/jgrd.50203

Sillmann J, Kharin VV, Zwiers FW, Zhang X, Bronaugh D (2013b) Climate extremes indices in the CMIP5 multimodel ensemble: part 2. Future climate projections. J Geophys Res Atmos 118(6):2473–2493. doi:10.1002/jgrd.50188

Taylor KE, Stouffer RJ, Ga Meehl (2012) An overview of CMIP5 and the experiment design. Bull Am Meteorol Soc 93(4):485–498. doi:10.1175/BAMS-D-11-00094.1

Tebaldi C, Hayhoe K, Arblaster JM, Ga Meehl (2006) Going to the extremes. Clim Change 79(3–4):185–211. doi:10.1007/s10584-006-9051-4

Teichmann C, Eggert B, Elizalde A, Haensler A, Jacob D, Kumar P, Moseley C, Pfeifer S, Rechid D, Remedio A, Ries H, Petersen J, Preuschmann S, Raub T, Saeed F, Sieck K, Weber T (2013) How does a regional climate model modify the projected climate change signal of the driving GCM: a study over different CORDEX regions using REMO. Atmosphere 4(2):214–236. doi:10.3390/atmos4020214

Vuuren DP, Edmonds J, Kainuma M, Riahi K, Thomson A, Hibbard K, Hurtt GC, Kram T, Krey V, Lamarque JF, Masui T, Meinshausen M, Nakicenovic N, Smith SJ, Rose SK (2011) The representative concentration pathways: an overview. Clim Change 109(1–2):5–31. doi:10.1007/s10584-011-0148-z